Redox Biology 11 (2017) 176–191

Contents lists available at ScienceDirect

Redox Biology

journal homepage: www.elsevier.com/locate/redox

Research Paper

Redox-guided axonal regrowth requires cyclic GMP dependent protein kinase 1: Implication for neuropathic pain

Lucie Valek[a], Annett Häussler[a], Stefan Dröse[b], Philipp Eaton[d], Katrin Schröder[c], Irmgard Tegeder[a,*]

[a] Depts. of Clinical Pharmacology, Goethe-University Hospital, Frankfurt, Germany
[b] Depts. of Anaesthesiology, Goethe-University Hospital, Frankfurt, Germany
[c] Depts. of Cardiovascular Physiology, Goethe-University Hospital, Frankfurt, Germany
[d] King's College of London, Cardiovascular Division, The Rayne Institute, St. Thomas' Hospital, London, United Kingdom

ARTICLE INFO

Keywords:
Sensory neuron
Nerve regeneration
Pain
Growth cone
Signaling ROS
Cofilin
Redox

ABSTRACT

Cyclic GMP-dependent protein kinase 1 (PKG1) mediates presynaptic nociceptive long-term potentiation (LTP) in the spinal cord and contributes to inflammatory pain in rodents but the present study revealed opposite effects in the context of neuropathic pain. We used a set of loss-of-function models for *in vivo* and *in vitro* studies to address this controversy: peripheral neuron specific deletion (SNS-PKG1$^{-/-}$), inducible deletion in subsets of neurons (SLICK-PKG1$^{-/-}$) and redox-dead PKG1 mutants. In contrast to inflammatory pain, SNS-PKG1$^{-/-}$ mice developed stronger neuropathic hyperalgesia associated with an impairment of nerve regeneration, suggesting specific repair functions of PKG1. Although PKG1 accumulated at the site of injury, its activity was lost in the proximal nerve due to a reduction of oxidation-dependent dimerization, which was a consequence of mitochondrial damage in injured axons. *In vitro*, PKG1 deficiency or its redox-insensitivity resulted in enhanced outgrowth and reduction of growth cone collapse in response to redox signals, which presented as oxidative hotspots in growing cones. At the molecular level, PKG1 deficiency caused a depletion of phosphorylated cofilin, which is essential for growth cone collapse and guidance. Hence, redox-mediated guidance required PKG1 and consequently, its deficiency *in vivo* resulted in defective repair and enhanced neuropathic pain after nerve injury. PKG1-dependent repair functions will outweigh its signaling functions in spinal nociceptive LTP, so that inhibition of PKG1 is no option for neuropathic pain.

1. Introduction

Peripheral nerve injury is a frequent cause of persistent neuropathic pain that may be interpreted as the result of multi-faceted adaptive processes gone wrong. Peripheral neurons have the inherent capacity to regrow and eventually re-innervate the target if the correct path is not lost, a prerequisite that depends on a complex network of guidance cues and intact myelin sheaths [1,2]. It is believed that successful re-innervation leads to pain resolution [3] whereas aberrant growth and sprouting increases pathological spontaneous activity and hyperexcitability [4,5]. But even on structural restitution, pain may persist as a consequence of functional or structural synaptic potentiation [6–8].

The induction of spinal long-term potentiation involves cGMP [9–11]. The process starts with activation of the NMDA receptor, subsequent activation of neuronal nitric oxide synthase (nNOS), nitric oxide (NO) production and activation of soluble guanylyl cyclase (sGC), finally producing cyclic GMP. cGMP also originates from natriuretic peptide/Npr signaling and regulates multiple cellular targets, including diverse cGMP-gated ion channels [12,13], the cGMP-dependent protein kinases, PKG1 and PKG2 [14,15], phosphodiesterases and cysteine rich protein 2 [16]. Nearly all of these molecular targets of cGMP are expressed in nociceptive pathways and potentially contribute to the key role of cGMP in synaptic scaling in the spinal cord [9–11].

Among these targets, PKG1 has emerged as a key mediator of

Abbreviations: ATF3, Activating transcription factor-3; ADF, Actin depolymerizing factor; cGMP, cyclic guonosine monophosphate; Cre, Cre recombinase; DRG, Dorsal root ganglia; EYFP, Enhanced yellow fluorescent protein; GAP43, Growth associated protein 43; IP3, Inositol trisphosphate; IRAK, Inositol trisphosphate receptor-associated cGMP-kinase substrate; H2O2, Hydrogen peroxide; NF200, Neurofilament of 200 kDa; NO, nitric oxide; NOS, nitric oxide synthase; Npr, Natriuretic peptide receptor; OXPHOS, Oxydative phosphorylation; PKG1, cGMP dependent protein kinase 1 (prkg1); ROS, Reactive oxygen species; sGC, soluble guanylyl cyclase; SLICK, Single neuron labeling with inducible cre-mediated knockout; SNI, Spared nerve injury; SNS, Tetrodotoxin-resistant sodium channel, Nav1.8; TAM, tamoxifen; TRPA1, Transient receptor potential channel subfamily A, type 1; TRPV1, Transient receptor potential channel subfamily V, type 1; Vasp, Vasodilator-stimulated phosphoprotein

* Corresponding author.
E-mail address: itegeder@hotmail.com (I. Tegeder).

http://dx.doi.org/10.1016/j.redox.2016.12.004
Received 13 July 2016; Received in revised form 3 November 2016; Accepted 2 December 2016
Available online 07 December 2016
2213-2317/

nociceptive signaling in inflammatory conditions [9,16–18]. The α-isoform of PKG1 is highly expressed in primary sensory neurons in the dorsal root ganglia (DRG) and in several regions in the brain and the spinal cord [16,17,19] and pharmacological and genetic studies have linked PKG1 to the development of nociceptive hypersensitivity and spinal mechanisms of inflammatory hyperalgesia [17].

PKG1 activation does not entirely depend on cGMP but also ensues on oxidative cysteine modification resulting in its dimerization and auto-activation [20,21]. This redox switch is particularly important in nociceptive neurons that mostly do not express sGC [16] and therefore may depend on oxidation-mediated PKG1 activation to maintain its function. PKG1 phosphorylates key regulators of intracellular calcium stores, namely the inositol 3-phosphate receptor [9] and its substrate (IRAG) [22], as well as effector molecules, which regulate the dynamics of actin and myosin [9,23,24]. These mechanisms are crucial for synaptic vesicle cycling and hence glutamate and neuropeptide release. As a consequence, PKG1 promotes inflammatory hyperalgesia and a specific loss of PKG1 in presynaptic compartments of the nociceptive synapse abolishes C-fiber-evoked long-lasting potentiation [9]. PKG1-mediated regulations of actin and myosin dynamics may also critically impact on regrowth and guidance of peripheral axons after injury, and injury-evoked redox imbalances may interfere with PKG1 dimerization and activity. As PKG1 has been suggested as a target for pain control, we asked if and how the complex functions of PKG1 affect neuropathic pain and repair after sciatic nerve injury.

2. Methods

2.1. Generation of neuron-specific PKG1 deficient mice

Mice lacking PKG1 specifically in primary nociceptive neurons were generated via Cre-loxP-mediated recombination by mating mice carrying the floxed *prkg1* allele ($PKG1^{fl/fl}$) [19] with a mouse line expressing Cre recombinase under control of the Nav1.8 promoter (SNScre) [25,26]. SNScre mice enable gene recombination commencing at birth selectively in Nav1.8-expressing sensory neurons of the dorsal root ganglia and trigeminal ganglia, without affecting gene expression at other sites [26,27]. We have shown that SNS-$PKG1^{-/-}$ have a specific deletion of PKG1 in the dorsal root ganglia but not in the spinal cord or brain [9]. Unlike global $PKG1^{-/-}$ mice [17], SNS-$PKG1^{-/-}$ mice show normal lamination of the spinal cord and have no developmental deficits [9]. To generate tamoxifen inducible PKG1-deficient mice in subsets of neurons we crossed the $PKG1^{fl/fl}$ mice with SLICK-X mice [28], which carry a double-headed Thy1-promoter, one head driving tamoxifen-inducible creERT expression and the other driving EYFP expression. Successful Cre-mediated excision of the *prkg1* allele was confirmed by PCR-based genotyping as described [19]. Genotyping for cre-recombinase used the primer: left: gaa agc agc cat gtc caa ttt act gac cgt ac; right: gcg cgc ctg aag ata tag aag a) and was done as described [29].

2.2. Mouse strains

Male and female 8–16 weeks old SNS-$PKG1^{-/-}$ and their $PKG1^{fl/fl}$ littermates were used for behavioral experiments, generation of primary DRG neuron cultures, western blotting and immunofluorescence studies. Tamoxifen versus vehicle treated SLICK-X-PKG1 mice were used to assess regrowth in vivo. The tamoxifen protocol consisted in once daily i.p. injection of 0.15 mg/gram of body weight for 5 consecutive days in 9:1 corn oil/ethanol followed by a free interval of 14 days before induction of the sciatic nerve lesion. The controls were littermates treated with vehicle (9:1 corn oil/ethanol). For analysis of redox sensitive growth cone collapse we used the DRG neurons of redox-dead Cys42Ser PKGI-alpha knock-in mice, in which the redox sensitive cysteine Cys42 has been replaced with a serine [20]. Mice had free access to food and water and were maintained in climate controlled rooms with a 12 h light-dark cycle. Behavioral experiments were performed between 10 am and 3 pm. The experiments were approved by the local Ethics Committee for animal research (Darmstadt, Germany), adhered to the guidelines for pain research in conscious animals of the International Association for the Study of PAIN (IASP) and those of the Society of Laboratory Animals (GV-SOLAS) and were in line with the European and German regulations for animal research.

2.3. Injury of the sciatic nerve

Surgery was performed under 1.5–2% isoflurane anesthesia plus local anesthesia of the skin. For the spared nerve injury (SNI) model of neuropathic pain, two of the three peripheral branches of the sciatic nerve, the common peroneal and the tibial nerves, were ligated and distally transected, leaving the sural nerve intact [30], which eventually sprout into denervated skin areas [5]. For the crush injury the exposed sciatic nerve was crushed for 30 s with a blunt, finely serrated 2 mm tip needle holder. The injury spares the myelin sheaths and allows for regrowth and re-innervation. Mechanical, heat and cold withdrawal latencies were recorded before the injuries and up to 4 weeks thereafter.

2.4. Behavioral experiments

The tests were performed by an investigator who was unaware of the mouse genotype and included 8–10 mice per group. Mice were habituated to the room and test chambers before the baseline measurement. The latency of paw withdrawal on pointy mechanical stimulation was assessed using a Dynamic Plantar Aesthesiometer (Ugo Basile, Comerio, Italy). The steel rod was pushed against the plantar paw with ascending force (0–5 g, over 10 s, 0.2 g/s) and then maintained at 5 g until the paw was withdrawn. The paw withdrawal latency was the mean of three consecutive trials with at least 30 s intervals.

To assess cold allodynia a drop of acetone was applied to the plantar ipsi-lateral hindpaw and the withdrawal response including paw lifting, shaking and licking was recorded with a stop watch for 90 s starting right after acetone application. The sensitivity towards cold was also assessed with a cold plate kept at 4 °C. Mice were put onto the plate and the number of withdrawal reactions including paw licking, lifting or shaking or jumping were counted during an observation period of 90 s, after which mice were returned to their home cage. Cold tests were done once per day.

The sensitivity to painful heat stimuli was assessed by recording the paw withdrawal latency with a Hot Plate (52 °C surface, Föhr Medical Instruments, Germany) or with the Hargreaves test (IITC Life Sciences). For the latter, a heating lamp was placed with a mirror system underneath the respective hind paw. By pressing the start button the lamp starts to emit a heat-beam until the paw is withdrawn, which stops the lamp. The mean paw withdrawal latency of three tests with at least 10 min intervals was used for statistical analysis.

Motor function was assessed with the accelerating RotaRod test (15–30 rpm, ramp 3 rpm/min, cut-off 5 min). Habituation encompassed 2–3 test runs. The fall-off latency was averaged from 2 tests. Behavioral tests were performed at baseline and 1, 3, 7, 14, 21 and 28 days after sciatic nerve injury. Exact time courses are shown in the respective figures.

2.5. Quantitative RT-PCR (QRT-PCR)

Total RNA was extracted from homogenized tissue according to the

protocol provided in the RNAeasy tissue Mini Kit (Qiagen, Hilden, Germany), and reverse transcribed using poly-dT as a primer to obtain cDNA fragments. QRT-PCR was performed on an ABI prism 7700 TaqMan thermal cycler (Applied Biosystems, Germany) using the SybrGreen detection system with primer sets and probes designed on the TaqMan software. Transcript regulation relative to the house-keeping gene, Gapdh was determined using the relative standard curve method according to the manufacturer's instructions (Applied Biosystems). Amplification was achieved at 59 °C for 35 cycles.

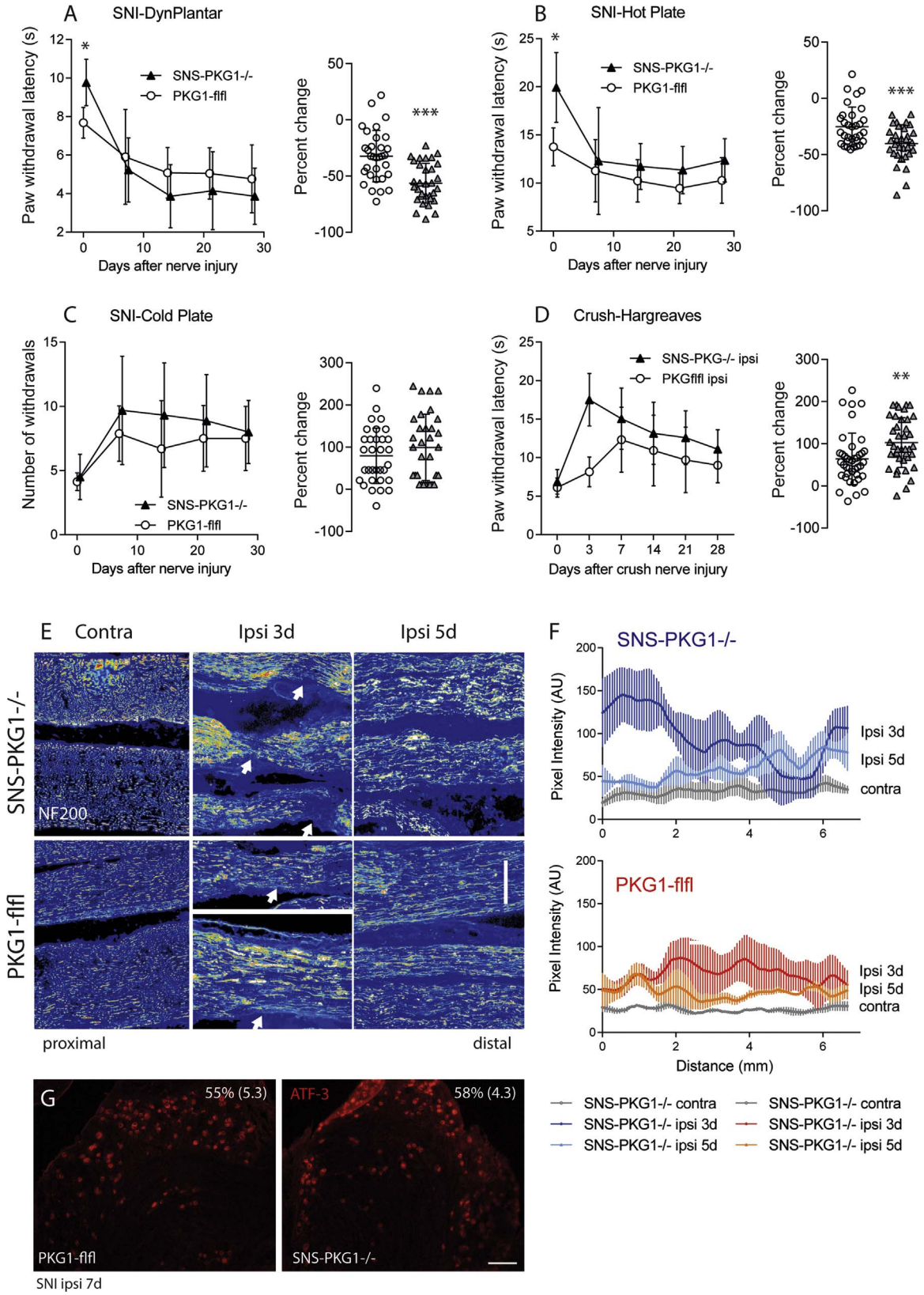

Fig. 1. Nociception, sensory functions and sciatic nerve morphology in SNS-PKG1$^{-/-}$ and PKG1$^{fl/fl}$ mice in the Spared sciatic Nerve Injury (SNI) and the Crush sciatic nerve injury models. A: paw withdrawal latencies and percentage change of PWLs on mechanical stimulation before and after SNI (n=8). The scatter plot shows the percentage change relative to baseline of all measurements 7, 14, 21 and 28 days after nerve injury, n=8 mice. * $P < 0.05$; *** $P < 0.001$; 2-sided, unpaired Student's *t*-test. Time courses were compared using ANOVA for repeated measurements (rm-ANOVA, between subject factor genotype, within subject factor time, $P < 0.05$). B: paw withdrawal latencies and percentage change of PWLs on heat stimulation (n=8). C: number of withdrawal reactions and percentage change on cold stimulation (n=8). D: paw withdrawal latencies and percentage change of PWLs on heat stimulation in the Hargreaves test after crush injury of the sciatic nerve (n=8). Because all fibers are injured in this model control mice show a temporary loss of sensory functions, particularly heat. ** $P < 0.01$; 2-sided, unpaired Student's *t*-test. E: reconstruction of long distances of the sciatic nerve 3 and 5 days after crush injury in PKG1$^{fl/fl}$ and SNS-PKG1$^{-/-}$ mice. The fibers were stained with neurofilament of 200 kDa (NF200) and the crush site is marked with white arrows. At 3d the hypo-dense gap was larger in SNS-PKG1$^{-/-}$ mice. At 5d injury sites were mostly "closed". F: ipsilateral and contralateral sciatic nerves of n=3 mice per genotype and time point were analyzed using profile plots (ImageJ). Data were exported, smoothed and plotted versus distance from proximal to distal. A drop of the intensity and pre- and post-lesion accumulations mark the site of injury. Profile plots and time courses differed significantly between genotypes, 2way-ANOVA $P < 0.05$. Scale bar 200 μm. G: ATF3 immunofluorescence of the ipsilateral L5 DRGs 7 days after SNI. The numbers of ATF3 positive neurons (means ± SD of n=4 mice) did not differ between genotypes. Scale bar 100 μm.

2.6. Western blot analysis

Protein extracts were prepared in PhosphoSafe Buffer (Sigma Germany) containing a protease inhibitor cocktail and PMSF 10 μg/ml, separated on 12 or 14% SDS-PAGE gel (30 μg protein/lane), transferred to nitrocellulose membranes (Amersham Pharmacia Biotech, Freiburg, Germany) by wet-blotting. Blots were blocked and developed in Odyssee buffer or 5% skim milk in 1xPBS/Tween 20. PKG1 was detected with an antibody directed against a C-terminal peptide of PKG1 (Abcam or Enzo KAP-PK005-D for dimer/monomer detection). Cofilin and phospho-cofilin antibodies were from Santa Cruz Biotechnology (rabbit pAb 1:200). β-actin (Sigma) or Hsp90 (Sigma) were used as loading controls. Secondary antibodies were conjugated with IRDye 680 or 800 (1:10000; LI-COR Biosciences, Bad Homburg, Germany) for detection and blots were analyzed on the Odyssey Infrared Imaging System (LI-COR Biosciences). The ratio of the respective protein band to the loading control was used for semi-quantitative analysis (Odyssee software).

For analysis of PKG1 dimer and monomer per Western Blot, mice were intracardially perfused with 0.5 mM N-ethylmaleimide (NEM) in saline for 10 min before excision of the tissue. Proteins were extracted under reducing (buffer containing DTT) or non-reducing conditions (no DTT) conditions and separated on SDS PAGE gels, followed by blotting, antibody incubation and detection as described above.

2.7. PKG1 activity

PKG1 activity was analyzed in ipsi and contralateral DRGs and sciatic nerves of 8 mice 3 days after crush injury of the sciatic nerve with the Cyclex activity assay according to the manufacturer's instructions. The assay uses a peroxidase coupled phospho-specific monoclonal antibody that recognizes the phospho-threonine 68/119 residues on G-kinase substrate, which is pre-coated to 96-well plates. PKG1 in the sample phosphorylates the substrate, which is detected with the antibody, followed by enzymatic conversion of the peroxidase substrate, tetra-methylbenzidine, and quantified by spectrophotometry at 450 nm.

2.8. Oxygraph analysis of mitochondrial OXPHOS activity

Mitochondrial respiration was assessed 2 h after nerve injury in tissue homogenates of ipsi and contralateral trigeminal and sciatic nerves and trigeminal and dorsal root ganglia. Tissue pieces of each 6 mice were pooled to get sufficient numbers of mitochondria for oxygraph measurements. Oxygen consumption was measured with an Oxygraph-2k (Oroboros, Innsbruck) at 30 °C in a buffer containing 200 mM sucrose, 10 mM Tris/HCl, 10 mM potassium phosphate, 10 mM $MgSO_4$, 2 mM EDTA, pH 7.0. After analysis of baseline respiration in the absence of exogenous substrates, the NADH-generating substrates 5 mM glutamate/5 mM malate (G/M) were added to initiate respiration via complex I. ADP was then added at a saturating level (2 mM) to maximally stimulate respiration in the presence of glutamate and malate. Subsequently, addition of 3 μM rotenone inhibited complex I, and respiration through complex II was initiated by adding 5 mM succinate. Finally, 2 mM KCN was added to completely inhibit mitochondrial respiration and to determine the mitochondria-independent oxygen consumption of the homogenate that was subtracted from all other rates. The 'coupling' of the mitochondria was determined by dividing the oxygen consumption in presence/in absence of ADP with G/M.

2.9. Immunofluorescence studies

Mice were terminally anesthetized with isoflurane and cardially perfused with cold 1xPBS, pH 7.4 followed by 4% paraformaldehyde in 1xPBS for fixation. Tissues were excised, postfixed in 4% PFA for 2 h, cryoprotected overnight in 20% sucrose at 4 °C, embedded in small tissue molds in cryo-medium and cut on a cryotome (10 or 12 μm for DRGs and sciatic nerves). Slides were air-dried and stored at −80 °C. After thawing, slides were immersed and permeabilized in 1xPBS with 0.3% Triton-X-100 (PBST), then blocked with 1% blocking reagent (Roche) or with 10% donkey or horse serum in PBST, subsequently incubated overnight with the first primary antibody in PBST at 4 °C. After washing slides were incubated with the secondary antibody for 3–4 h at room temperature. The procedure was repeated for the second primary/secondary antibody pair, followed by 30 min incubation with DAPI (in some experiments) and embedding in Fluoromount. The general settings were optimized for the respective antibodies and tissues. Primary antibodies included PKG1 (Genway, Enzo), EGFP-FITC (Abcam), ATF3 (SantaCruz), NF200 (Sigma), GAP43 (Chemicon) and ERAB (mitochondria, Abcam) and are listed in Suppl. Table 1. ATF3 is a marker for neurons with axonal injury [31] and GAP43 detects regenerating neurons [32]. Phalloidin-Alexa-594 (lifetechnologies) was used for staining of F-actin. Secondary antibodies were labeled with fluorochromes or IR dyes (Invitrogen, Sigma, Chemicon).

Slides were analyzed on an inverted fluorescence microscope (Axio Imager Z1, Zeiss, Germany). Tiled images were captured to cover the full length of the sciatic nerve from proximal to distal of the lesion and stitched. The length and area of the lesion was analyzed with FIJI ImageJ. After subtraction of the background and auto-threshold setting with minor adjustments the rectangle selection tool was used to define the region of interest representing the full length of the nerve. The profile plot (intensity versus distance data) of this ROI was exported to SigmaPlot 12.5, smoothed using the Reverse Exponential algorithm and the area under the curve calculated with the linear trapezoidal rule. The AUCs were statistically compared. The intensities of the nerves are presented as Rainbow pseudocolor (some experiments). The numbers of ATF3 positive and GAP43 positive DRG neurons were counted relative to the number of all neurons in the section.

JC-1 (lifetechnologies) immunostaining was used to assess the

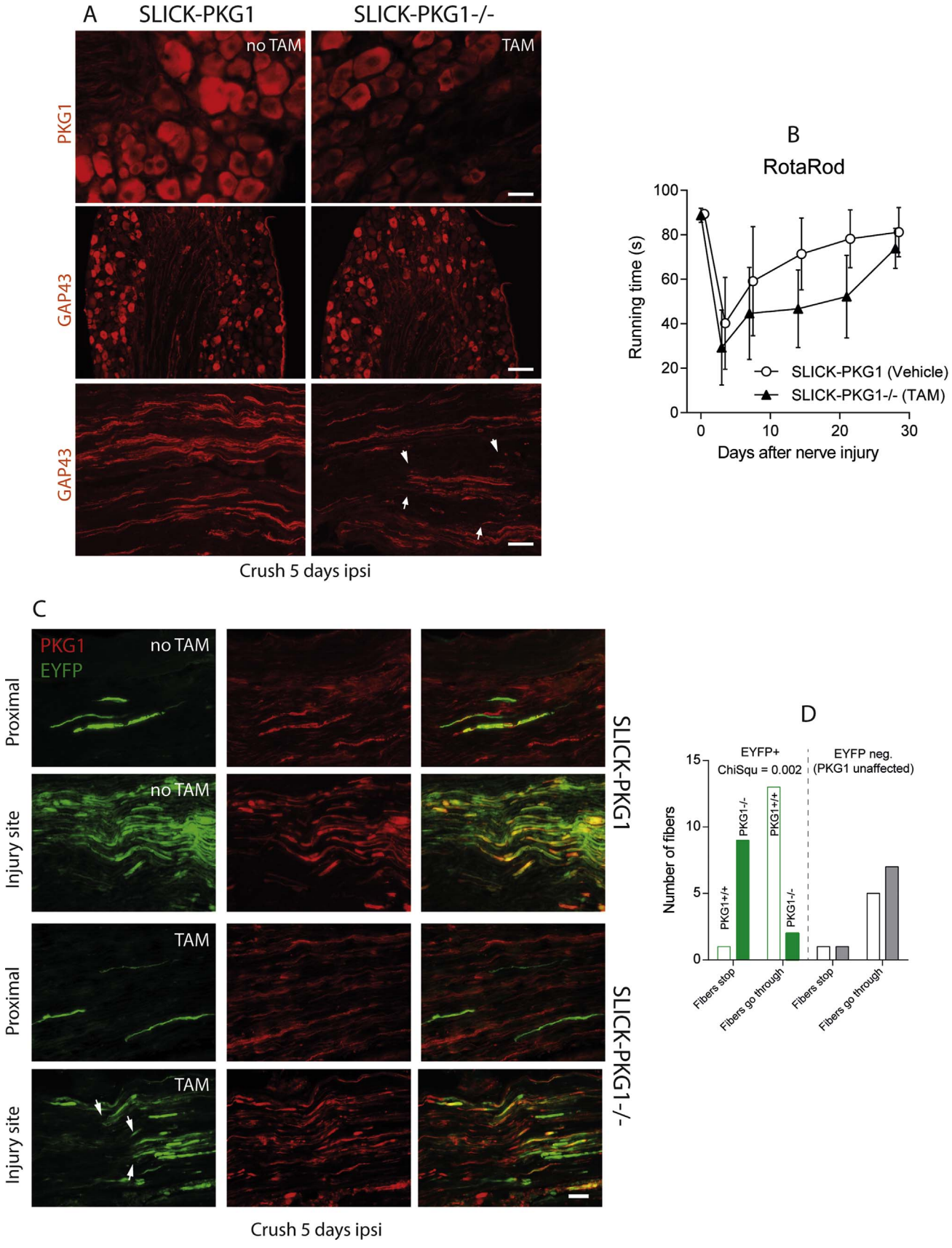
A
SLICK-PKG1
SLICK-PKG1-/-
no TAM
TAM
PKG1
GAP43
GAP43
Crush 5 days ipsi
B
RotaRod
Running time (s)
100
80
60
40
20
0
0
10
20
30
Days after nerve injury
SLICK-PKG1 (Vehicle)
SLICK-PKG1-/- (TAM)
C
PKG1
EYFP
no TAM
Proximal
Injury site
no TAM
TAM
Proximal
TAM
Injury site
SLICK-PKG1
SLICK-PKG1-/-
Crush 5 days ipsi
D
EYFP+
ChiSqu = 0.002
EYFP neg.
(PKG1 unaffected)
Number of fibers
15
10
5
0
PKG1+/+
PKG1-/-
PKG1+/+
PKG1-/-
Fibers stop
Fibers go through
Fibers stop
Fibers go through

Fig. 2. Immunofluorescence analysis of axonal regrowth after crush injury in SLICK-X-PKG1 mice. A: immunofluorescence analysis of PKG1 and GAP43 in the DRGs and sciatic nerve 5 days after crush injury in SLICK-PKG1 mice treated with tamoxifen (SLICK-X-PKG1$^{-/-}$) or vehicle (SLICK-X-PKG1). Top: tamoxifen treatment resulted in PKG1 deletion in subsets of DRG neurons. Vehicle treated mice (noTAM) were the controls. Middle and bottom panels show GAP43, which is a marker for regenerating axons. In tamoxifen treated SLICK-PKG1$^{-/-}$ mice some GAP43 positive fibers stopped in front of the lesion (white arrows). The number of GAP43 positive DRG neurons did not differ between TAM versus vehicle treated mice. Results of 4 mice per group. Scale bar in 25 (DRGs) and 100 μm (nerve). B: RotaRod running times before and after Crush of the sciatic nerve in tamoxifen treated SLICK-PKG1$^{-/-}$ versus vehicle treated SLICK-PKG1 mice (n=8). C: immunofluorescence analysis of PKG1 and EYFP in the sciatic nerve 5 days after crush injury in SLICK-PKG1 mice treated with tamoxifen (SLICK-PKG1$^{-/-}$) or vehicle. Tamoxifen treatment resulted in PKG1 deletion in creERT positive neurons, which were identified via their EYFP expression. In vehicle treated SLICK-PKG1 mice (noTAM) EYFP and PKG1 overlap (yellow fibers). After tamoxifen treatment EYFP and PKG1 are mostly mutually exclusive showing tamoxifen-induced PKG1 deletion in EYFP positive fibers. The green PKG1 deficient fibers in the tamoxifen group stopped in front of the lesion whereas most fibers grew through the gap in the vehicle treated group. Results of 4 mice per group. Scale bar 100 μm. D: frequency distribution of PKG1 positive and PKG1 negative fibers, which grew through or stopped in front of the lesion. Fibers were counted and compared with Chi Square statistics. $P < 0.05$. (For interpretation of the references to color in this figure legend, the reader is referred to the web version of this article.)

mitochondrial membrane potential. The dye exists either as a green-fluorescent monomer at depolarized membrane potentials or as a red fluorescent J-aggregate at hyperpolarized membrane potentials. Mitochondrial damage or loss of membrane potential is indicated by a decrease of the red/green ratio. Tissue sections were permeabilized in PBS-0.05% Tween for 20 min, blocked for 30 min in 10% BSA/PBS-0.05% Tween 20, followed by incubation with JC-1 (1:500) for 20 min at 37 °C in 1%BSA/PBS-0.05% Tween-20. After washing slides were imbedded and mitochondria were visualized by epifluorescence microscopy. Intensity plots were obtained along the full reconstructed nerves as described above and red-to-green ratios were plotted versus distance. For all quantifications 3–4 non-overlapping sections per mouse of each 3–4 mice per genotype were used.

2.10. Culture and staining of primary DRG neurons

Primary adult dissociated DRG neuron-enriched cultures were prepared by dissecting mouse DRGs into HBSS (Ham's balanced salt solution, Dulbecco) and 10 mM HEPES, followed by digestion with 5 mg/ml collagenase A and 1 mg/ml dispase II (Roche Diagnostics, Mannheim, Germany) prior to treatment with 0.25% trypsin (GibcoBRL, Karlsruhe, Germany). Triturated cells were centrifuged through a 10% BSA solution prior to plating on poly-L-lysine and laminin coated cover slips in Neurobasal medium (GibcoBRL) containing 2% (vol/vol) B27 supplement (GibcoBRL), 50 μg/ml Pen-Strep, 100 ng/ml NGF and 200 mM L-glutamine. After incubation for 2 h, 2 ml Neurobasal medium was added and neurons were incubated for 2 days or 7 days depending on the experiment with half exchange of the medium at 3 days. Cells were kept at 37 °C, 5% CO_2, 95% humidity.

After 48 h, neuron cultures were treated with 100 μM H_2O_2 (H_2O_2 30%, ROTH) for 0, 30 and 60 min. After the treatment, neuron cultures were washed in PBS, fixed in 4% PFA in 1xPBS and immunostained with NF200 and subsequent Cy3- or Alexa-488 labeled secondary antibodies and with phalloidin-Alexa-594 or PKG1 (Enzo, Genway). Images were captured on an inverted Axio Imager Z1 fluorescence microscope (Zeiss, Jena, Germany). The quantification of neurite outgrowth was done with the autmess modul of AxioVision 4.2 (Zeiss), adjusted for shading and automatic detection of cell soma and neurites. The area covered by cell bodies plus neurites relative to the total area of the image was used for quantification and statistical comparison. For analysis of neurite branching FIJI ImageJ was used. After subtraction of background a binary image was generated and subsequently analyzed with the segmentation tool using auto-settings. The average and total length of the branches, number of junctions, triple and quadruple joints were compared with GraphPad Prism 6.

The co-dependent or random nature of apparent colocalizations was tested using the 'Intensity Correlation Analysis' (ICA) that generates ICA plots, PDM maps (product of the differences from the mean) and Intensity Correlation Quotients (ICQ). Further analyses included calculation of the Pearson's Correlation coefficient, R [33], Manders' colocalization coefficients M1 & M2 and Coste's automatic threshold method. The analysis is bundled with the JACoP plugin of FIJI ImageJ [34] and was performed with standard settings.

Growth cones were counted and qualified as spiky or collapsed or in between and numbers were compared with Chi Square statistics. The analyses are based on 12–16 cultures of 3–4 mice per genotype.

For detection of sites of oxidation neurons were fixed after 48 h in culture as described above and then labeled with 5 mM dimedone in 0.5% saponin for 1 h at room temperature. Dimedone specifically traps sulfenic acids, which are formed as transient intermediates on oxidation of susceptible cysteine residues in proteins, therefore allowing in situ detection of oxidation [35]. Neurons were then permeabilized and blocked in 2% horse serum, 2% methanol, 0.5% saponin in 1xPBS for 30 min and subsequently incubated with anti-cysteine sulfenic acid antibody (Millipore) at 4 °C overnight, washed, incubated with Alexa488 labeled secondary antibody and analyzed per fluorescence microscopy as described above. Alternatively, cysteine sulfenic acid probe (DCP-Bio1, EMD Millipore) was used. It consists of the sulfenic acid-reactive 3-(2,4-dioxocyclohexyl) propyl (DCP) appended to biotin and was detected with streptavidin-Alexa488 or streptavidin-HRP.

2.11. Statistics

SPSS 23.0 was used for statistical evaluation. Data are presented as means ± SD unless indicated otherwise. Behavioral data were analyzed using ANOVA for repeated measurements for time courses and one-way ANOVA or *t*-tests to compare areas under the curve. The latter were calculated according to the linear trapezoidal rule. Counts of neurons, QRT-PCR and western blot results were analyzed with Student's *t*-tests (for two groups), one-way ANOVA or ANOVA for repeated measurements (rm-ANOVA). *P* was set at 0.05 for all statistical comparisons. In case of multiple comparisons, we used a correction of alpha according to Bonferroni. Numbers of growth cones and fibers were compared with Chi Square statistics. The numbers of animals and test replicates are indicated in the respective figure legends.

3. Results

3.1. Nerve injury evoked nociception in SNS-PKG1$^{-/-}$ mice

Nociception of SNS-PKG1$^{-/-}$ mice was analyzed in comparison with littermate control mice (PKG1$^{fl/fl}$) in two models of neuropathic pain, the Spared Nerve Injury (SNI) model and the Crush model. The SNI model causes nociceptive hypersensitivity because the sural nerve remains intact. In contrast, the crush model causes a temporary loss of sensitivity but allows for regeneration. At baseline SNS-PKG1$^{-/-}$ mice were less sensitive to mechanical or noxious heat stimulation (Fig. 1A, B). The protection was lost after nerve injury and the relative drop of the thresholds was stronger in the knockouts (Fig. 1A, B). Similarly, but

not significant SNS-PKG1$^{-/-}$ mice had a mildly stronger SNI-evoked response to cold, i.e. cold allodynia (Fig. 1C) and after Crush, SNS-PKG1$^{-/-}$ mice had a stronger and longer lasting loss of heat sensitivity (Fig. 1D). Hence, overall SNS-PKG1$^{-/-}$ mice showed stronger behavioral manifestations of nerve injury evoked sensory disturbances. In agreement with the behavior, fiber regrowth in crush injured sciatic

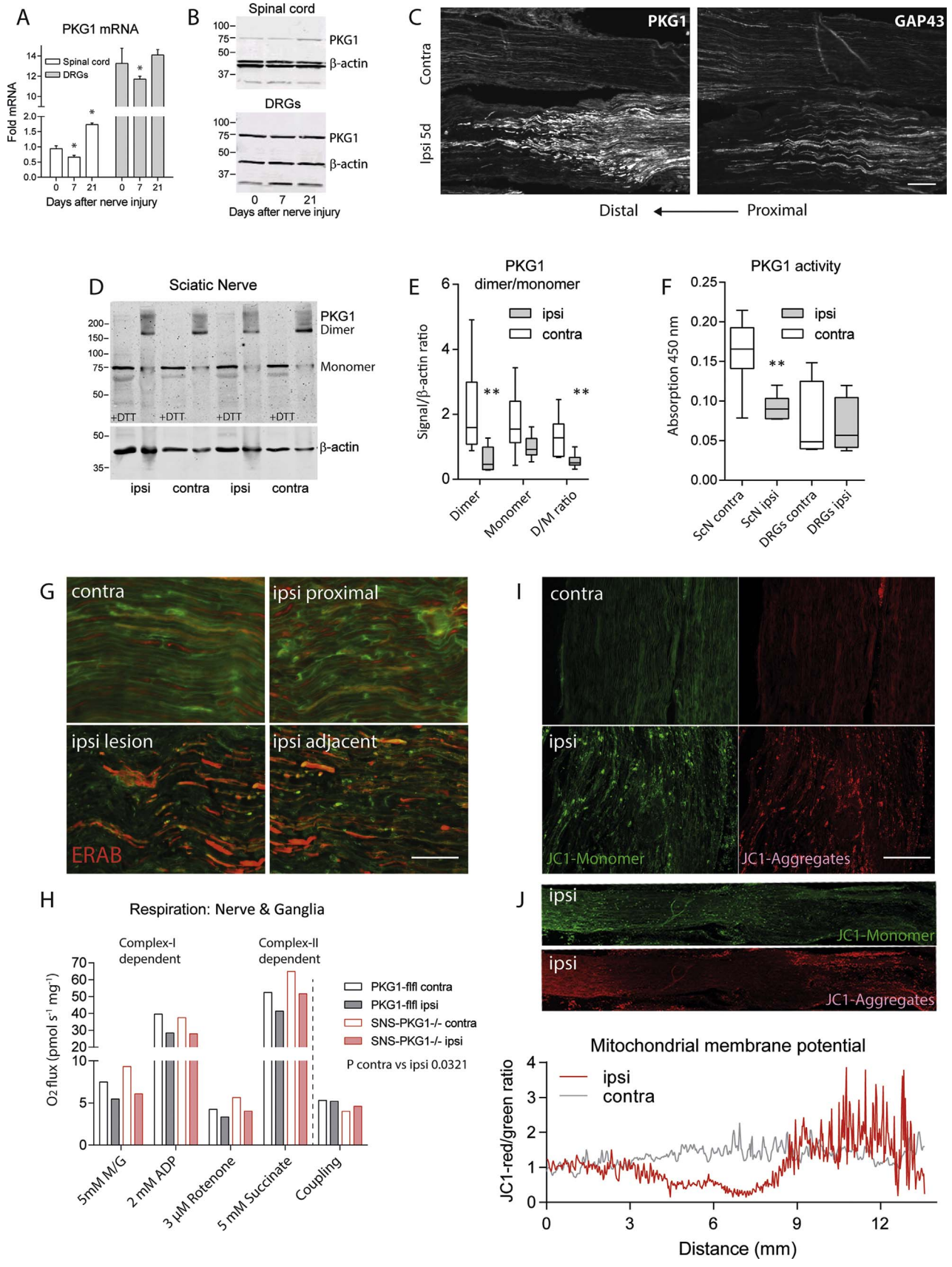

Fig. 3. PKG1 expression, axonal transport and mitochondrial functions after injury of the sciatic nerve. A: RT-PCR analysis of PKG1 in the ipsilateral spinal cord and DRGs in naïve mice (N) and after SNI (n=4 per genotype and time point, *P < 0.05 versus naive). B: western Blot of monomeric PKG1 in the spinal cord and DRGs in naïve mice and after SNI, representative result of n=3 per genotype and time point. C: immunofluorescence analysis of PKG1 and GAP43 in the contra and ipsilateral nerves at the site of the crush lesion showing the accumulation of PKG1 in front of the lesion. D: western Blot of PKG1 dimer and monomer in the ipsi and contralateral sciatic nerve 3 days after crush injury. Dimer and monomer were detected under non-reducing (without DTT) or reducing (with DTT) conditions, respectively. β-actin was used as loading control and signal to actin ratios were used for quantification. The blot shows a representative result of 8 mice. E: quantification of the Western Blot results shown in D. **P < 0.01, ANOVA, posthoc 2-sided, unpaired *t*-test between groups (n=8 mice per group) for dimer and monomer. F: PKG1 activity in contra and ipsilateral sciatic nerves and DRGs 3 days after crush injury. **ANOVA P < 0.01, posthoc 2-sided, unpaired *t*-test between groups (n=8 mice per group) for ScN and DRGs. G: immunofluorescence analysis of mitochondrial hydroxyacyl-CoA dehydrogenase (ERAB-red, fiber counterstain in green) in the crush-injured sciatic nerve, compared with the contralateral nerve. Damaged mitochondria accumulated at the site of the injury and the architecture was disturbed in the proximal nerve. Scale bar 100 μm. H: oxygraph analysis of mitochondrial respiration in ipsi- and contralateral nerves plus ganglia after injury of the nerve. The trigeminal nerve and ganglia were used in this experiment because of higher numbers of mitochondria. Data are of 8 animals per group (pooled samples) and compared per Chi Square statistics. P < 0.05. I: immunofluorescence analysis of JC-1 monomers and aggregates showing loss of the mitochondrial membrane potential in ipsilateral nerves 3 days after crush injury. Scale bars 150 μm. J: quantitative analysis of JC-1 immunofluorescence along the nerve using rectangle profile plots (ImageJ). Ratios of the red (aggregate) and green (monomer) intensities were smoothed and plotted versus distance from proximal to distal. A drop of the ratio marks the site of injury. (For interpretation of the references to color in this figure legend, the reader is referred to the web version of this article.)

nerves of SNS-PKG1$^{-/-}$ mice was protracted, which manifested with a longer hypo-dense gap at 3 days and stronger accumulation of neurofilament at the proximal border of the lesion (Fig. 1E, quantification 1 F). Both genotypes had similar numbers of ATF3 positive neurons in the DRGs, which is a marker for axonal injury (Fig. 1G, SNI).

3.2. Fiber regrowth in the crush injury model in SLICK-PKG1$^{-/-}$ mice

To further assess and confirm *in vivo* differences of nerve regeneration we used an additional model, in which PKG1 is knocked out upon tamoxifen treatment in subsets of neurons using SLICK-X-CreERT as the Cre-driver [28]. SLICK-X-CreERT have a tamoxifen-sensitive CreERT under control of a double headed Thy1 promoter, one driving CreERT and the other EYFP expression. Hence, all neurons with the capability to knockout PKG1 on tamoxifen treatment are green. The SLICK-PKG1$^{-/-}$ mice allow observation of PKG1 positive and negative fibers in the same mouse and also eliminate putative developmental influences.

We confirmed the successful Cre-loxP mediated recombination and reduction of PKG1 expression in the DRGs after tamoxifen (TAM) treatment in the DRGs (Fig. 2A, top). Upregulation of the regeneration marker GAP43 in the DRGs was similar in both genotypes (Fig. 2A middle). However, in the tamoxifen treated group, a higher number of GAP43 positive fibers broke off in front of the crush site (Fig. 2A bottom, arrows) and tamoxifen treated SLICK-X-PKG1$^{-/-}$ had a subtle impairment of the recovery of RotaRod running after crush injury (Fig. 2B).

Analysis of PKG1 and EYFP in the sciatic nerves of tamoxifen (SLICK-X-PKG1$^{-/-}$) versus vehicle treated SLICK-PKG1 mice confirmed that PKG1 was present in EYFP positive fibers without tamoxifen but rarely after tamoxifen treatment (Fig. 2C), i.e. PKG1 positive red fibers and EYFP positive green fibers were mutually exclusive after tamoxifen treatment. Because of the accumulation of both proteins this was most distinct in the proximal nerve. After crush injury both EYFP and PKG1 accumulated in front of the lesion. Without tamoxifen there were several double labeled fibers (i.e. PKG1+), most of them advancing through the lesion (Quantification Fig. 2D). After tamoxifen treatment, PKG1 negative fibers (green but not red) mostly stopped in front of the lesion. This was only evident in the EYFP+/PKG1- fibers. Hence, PKG1 deficient fibers failed to grow through the lesion. Basically, this may have 2 reasons, either PKG1 deficient fibers fail to extend or they fail to collapse. Both will hinder guidance through the lesion.

3.3. Nerve injury evoked regulation and axonal transport of PKG1 and its activators

The data in Figs. 1 and 2 suggested that PKG1 has repair functions after nerve injury. To address this function, we first analyzed its transcriptional and posttranslational regulation after nerve injury. After SNI PKG1 mRNA was temporarily decreased in DRGs and spinal cord around 7d followed by a re-raise at 21d (Fig. 3A). This time course was mildly reflected at the protein level of the PKG1-monomer (Fig. 3B). The block of axonal transport after injury caused an accumulation of PKG1 in front of the injury (Fig. 3C), which was further revealed by a double suture nerve constriction model (Suppl. Fig. 1). PKG1 accumulated in front of the proximal and somewhat weaker behind the distal suture suggesting a bidirectional transport in the intact nerve. The accumulation in front of the lesion was associated with an overall loss of PKG1 in the nerve, particularly of the active redox-dependent dimer (Fig. 3D, E). The stronger loss of the dimer as compared to the monomer indicates a reduction of oxidation-dependent disulfide formation and hence, loss of auto-activation, likely due to a loss of signaling ROS in close vicinity of PKG1. Consequently, PKG1 activity in the ipsilateral nerve was reduced (Fig. 3F). The major source of signaling ROS in the intact nerve are intact mitochondria. After nerve injury, morphologically damaged mitochondria accumulated in front of the lesion (Fig. 3G), mitochondria had reduced OXPHOS activity proximal of the lesion (Fig. 3H) and reduced membrane potentials along the nerve (Fig. 3I, quantification 3 J) suggesting that the generation of signaling ROS leading to PKG1 dimerization was reduced. This does not contradict a previously observed upregulation of pro-oxidative enzymes in the DRGs [36] or ROS production by infiltrating immune cells around the lesion.

Oxidation mediated activation of PKG1 likely is a major determinant of its activity in the nerve because the canonical NO-sGC/cGMP-PKG1 activation pathway is not functional in DRG neurons, which do not express soluble guanylyl cyclase (sGC) [16] and only some have nNOS [31]. We therefore focused on redox-dependent functions of PKG1 for outgrowth and repair.

3.4. Outgrowth of DRG neurons, oxidative hot spots and growth cone morphology

We assessed ROS-signals upon outgrowth of neurites in primary neuronal cultures employing dimedone trapping of sulfenic acids. Indeed, oxidative hot spots occurred at the growth cones and branching points (Fig. 4A), which reveal oxidative protein modifications [37]. Such oxidation points at growing tips impose a redox switch of actin polymerization [38,39] inducing growth cone collapse [40,41]. Dimedone hot spots in outgrowing cultures were somewhat more

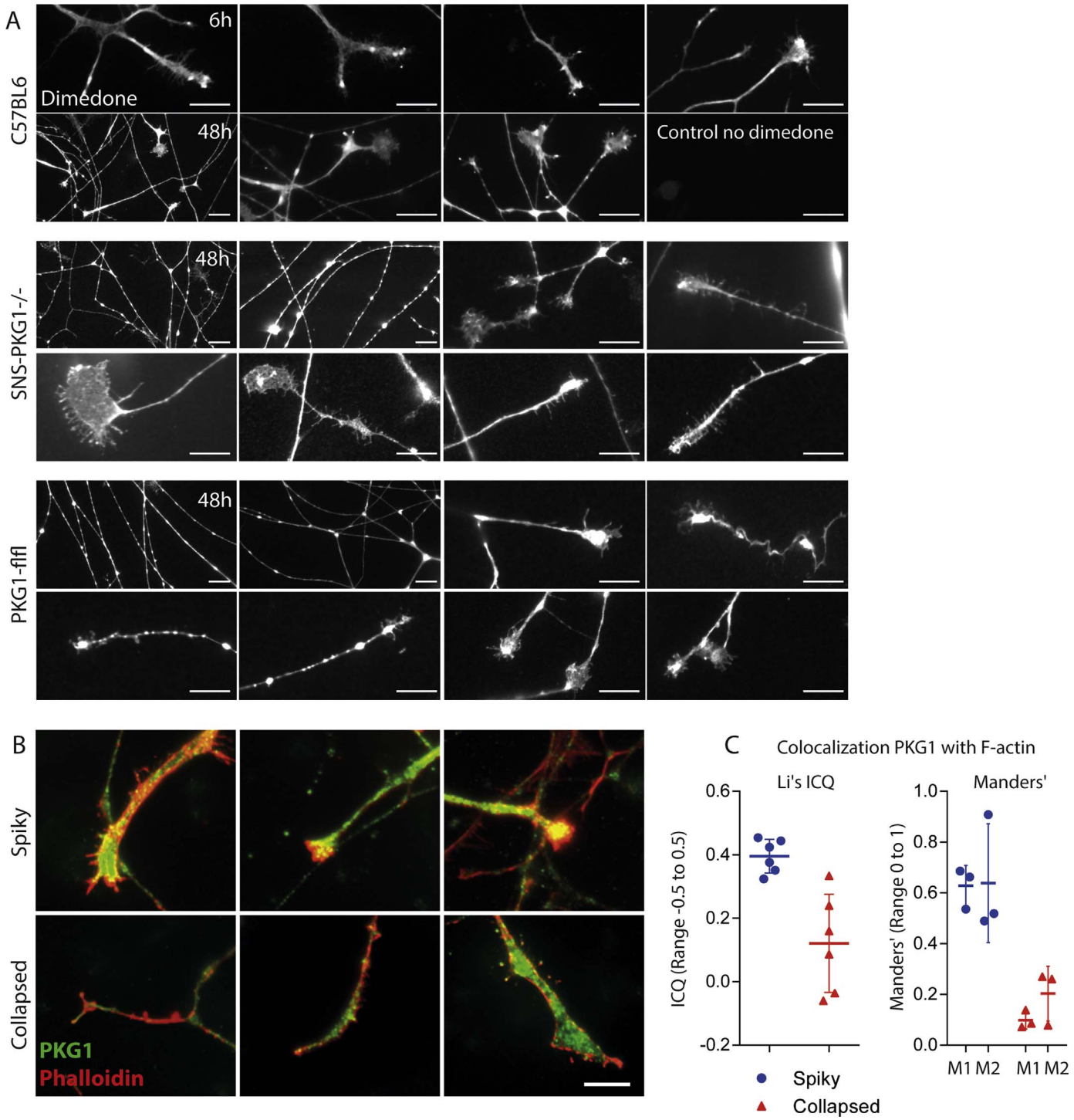

Fig. 4. Immunofluorescence analysis of the morphology, oxidation and PKG1 immunofluorescence in the growth cones of primary sensory neurons of the dorsal root ganglia of adult PKG1^{flfl} and SNS-PKG1$^{-/-}$ mice. A: exemplary images of dimedone labeling of protein sulfoxides marking oxidation hot spots in the growth cones and branching points in wild type DRG cultures, and in cultures of SNS-PKG1$^{-/-}$ and PKG1^{flfl} neurons 48 h after plating. SNS-PKG1$^{-/-}$ neurons showed a higher number of oxidative hot spots per neurite length (12/100 µm) than control neurons (7/100 µm). Scale bars 10 µm. B: PKG1 immunofluorescence in spiky and collapsed growth cones (each 3 examples) of wild type mice 48 h after plating. Phalloidin-Alexa549 was used to counterstain F-actin. Scale bars 10 µm. C: the co-dependent nature of PKG1 and phalloidin immunofluorescence was analyzed with the JaCoP2 Plugin of FIJI ImageJ. The scatter plots show Li's intensity correlation quotients (ICQ) and Manders' colocalization coefficients. Li's ICQ ranges from −0.5 (complete segregation), to 0.5 (complete colocalization). Zero means random coincidences. Manders' M1 shows overlap of channel A (Phalloidin) with channel B (PKG1) and M2 shows the reverse. M1 and M2 range from 0 (segregation) to 1 (complete colocalization). The analyses employed thresholds to define the cones as ROIs and exclude the surrounding area. Results in detail are presented in Suppl. Table 2.

frequent in SNS-PKG$^{-/-}$ cultures (~12/100 µm of neurite length versus ~7/100 µm in controls; Fig. 4A) suggesting that PKG1 was required at these sites to respond. Indeed, PKG1 immunofluorescence was very bright in spiky growing cones as described before [42] and colocalized here with F-actin (Fig. 4B). On collapse, PKG1 appeared to redistribute resulting in a decrease of its colocalization with F-actin (Fig. 4B, C; quantitative colocalization in Suppl. Table 2).

We therefore further analyzed growth cone morphology (Fig. 5) and outgrowth (Fig. 6) at a quantitative level. Growth cones of wild type PKG1^{flfl} DRG neurons showed a higher fraction of the collapsed

phenotype (36.5 ± 7%) as compared to SNS-PKG1$^{-/-}$ cultures (10.5 ± 4%), in which the spiky morphology predominated (Fig. 5 A,B, frequency distribution Fig. 5C). To specifically address the redox-dependent nature of this difference we repeated the experiment with redox-dead Cys42Ser PKG1 mutant neurons versus wild type and basically got the same result (Fig. 5D, E; Suppl. Fig. 2). Collapsed

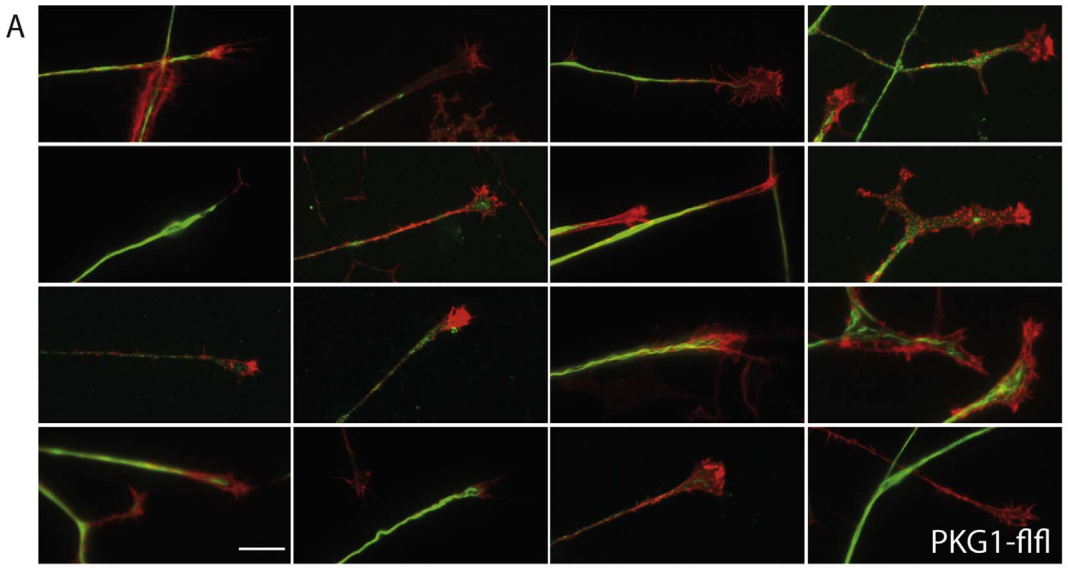

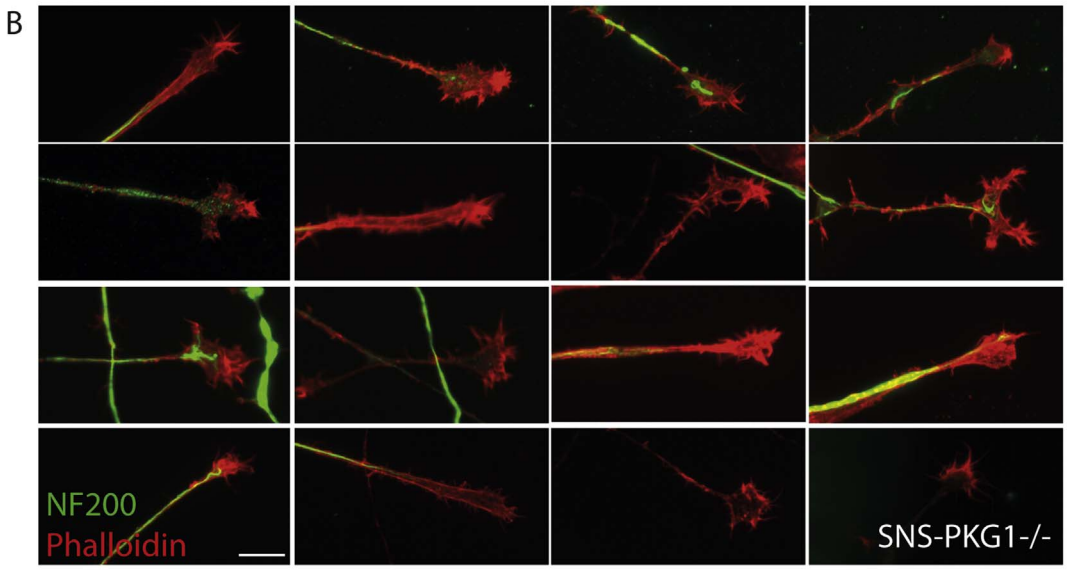

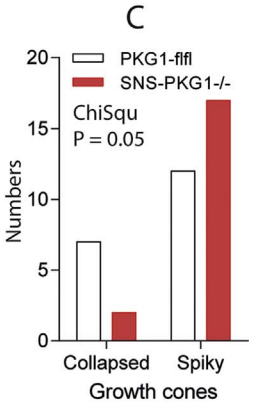

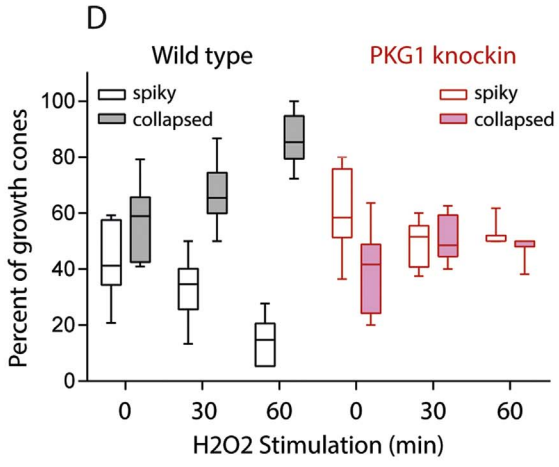

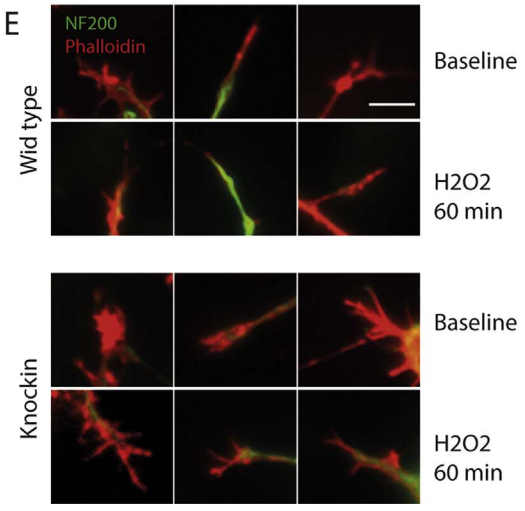

Fig. 5. Growth cone morphology of DRG neurons of PKG1 deficient versus control mice and of Cys42Ser PKG1 redox dead mutant versus wild type mice. A, B: exemplary growth cones of adult naïve PKG1$^{fl/fl}$ and SNS-PKG1$^{-/-}$ mice. Axons and neurites were stained with neurofilament of 200 kDa (NF200) and F-actin with phalloidin-Alexa594. Scale bar 10 μm. C: frequency distribution of spiky and collapsed growth cones of PKG1$^{fl/fl}$ and SNS-PKG1$^{-/-}$ neurons. The growth cones (n=20 per genotype) were categorized according to their morphology as spiky (growing), collapsed and in between. Counts of cones with intermediate morphology were similar and are not shown. Chi-Square analysis of the numbers of collapsed and spiky growth cones revealed significant differences. Cultures of 3–4 mice per genotype were analyzed. D: box plots showing the percentages of spiky and collapsed growth cones per slice culture of Cys42Ser redox dead PKG1 mutant neurons versus wild type neurons 24 h after plating. Neurons were stimulated for 0, 30 or 60 min with 100 μM H_2O_2. The box represents the interquartile range, the whiskers show minimum to maximum and the line is the median. E: exemplary images of redox dead PKG1 mutant neurons versus wild type neurons at baseline and at 60 min H_2O_2. A larger panel of cones is presented in Suppl. Fig. 2. 100 cones were counted and categorized per genotype and time point. Wild type cones collapsed under H_2O_2, whereas PKG1 mutant cones were largely resistant to this stimulus. The frequency distribution differed significantly between genotypes (Chi Square statistics, $P < 0.001$).

growth cones were less frequent in Cys42Ser PKG1 mutant cultures at baseline, and they were resistant to hydrogen peroxide evoked growth cone collapse. As a consequence of the reduction of redox-mediated growth cone collapse we found that the outgrowth of SNS-PKG1$^{-/-}$ neurons was enhanced as compared to the PKG1$^{fl/fl}$ controls (Fig. 6 A–C) resulting in stronger dendritic networks. Again, Cys42Ser PKG1 mutant cultures revealed similar but milder differences (Fig. 6D,E; Suppl. Fig. 3). Average and total neurite length were increased with Cys42Ser PKG1 mutant neurons, whereas junctions and quadruple points were reduced. Branching points occur upon resuming outgrowth after pausing [43]. Hence, reduced quadruple points suggested that the growing neurite paused less frequently. In summary, PKG1 deficiency or redox-unresponsiveness resulted in an impairment of oxidation-dependent growth cone collapse.

3.5. PKG1-dependent phosphorylation of cofilin

To assess underlying molecular mechanisms, we focused on the actin severing/depolymerizing protein cofilin because the localization studies (Fig. 4) had revealed a close association of PKG1 with F-actin in growing cones suggesting that PKG1 may be involved in actin remodeling. It has been shown that growth cone collapse induced by Sema3A and/or oxidation requires inactivation i.e. phosphorylation of cofilin [44], which is critical for axon extension and repulsion in dorsal root ganglia neurons [45]. We found a substantial reduction of cofilin phosphorylation in the sciatic nerve, DRGs and spinal cord in SNS-PKG1$^{-/-}$ mice both ipsi- and contralateral (Fig. 7) showing that its phosphorylation leading to inactivation critically depended on PKG1. The result supports the idea that cofilin is a PKG1-effector molecule. The PKG1-cofilin path is likely contributed by or is acting downstream of other cytoskeletal effector molecules that have been identified as PKG1 phosphorylation targets including vasodilator proteins (Ena/Vasp) [46,47] and myosin light chain (MLC) [9], which all converge on the regulation of microtubule and actin dynamics. PKG1 appears to be in the center of this complex regulatory network (Fig. 8).

4. Discussion

We show in the present study that PKG1 deficiency in injured neurons impairs regeneration of the sciatic nerve after injury leading to an enhancement of neuropathic pain behavior. PKG1 deficient axons failed to grow through the lesion likely because they were unable to correctly respond to redox-dependent repulsion cues required for pathfinding. We infer the latter from studies in primary DRG neurons: PKG1 deficient neurons and redox-dead PKG1 mutant neurons both showed enhanced outgrowth and a reduction of growth cone collapse, suggesting that oxidation-evoked PKG1 dimerization, which causes its auto-activation [20] was needed for redox-dependent repulsion. In line with the *in vitro* studies, PKG1 dimerization and activity were reduced *in vivo* because the injury caused mitochondrial damage resulting in a reduction of mitochondrial respiration and loss of membrane potential in injured axons. Mitochondria account for a great proportion of signaling ROS in axons so that their dysfunctions well explain the observed loss of PKG1's dimerization and activity.

Mechanistically, we show that PKG1 was necessary for the phosphorylation of ADF/cofilin in DRGs, spinal cord and sciatic nerve. P-cofilin leads to depolymerization of F-actin, an event that is crucial for oxidation-evoked growth cone collapse [44]. The phosphorylation of cofilin may be direct or mediated through Lim kinase [48], which is a PKG1 target [24] and the only kinase known so far to phosphorylate cofilin [49]. PKG1 also phosphorylates other key regulators of actin-myosin dynamics including Ena/VASP [46,47] and myosin light chain [9,50] either directly or through activation of upstream kinases or small G-proteins of the Rho family [47,51] (Fig. 8), which are all involved in the response to repulsion and attraction cues. Hence, PKG1 is strategically well positioned to act as a key second messenger for a number of guiding molecules.

Based on our results we propose a model, in which a redox signal generated in the growth cone attracts PKG1 to the cone, causes its oxidation-dependent dimerization and activation, which in turn phosphorylates cofilin thereby causing the cone to collapse and the redox signal to be switched off. On collapse, PKG1 retracts from the cone and the cycle would restart with the next attraction cue, which would again elicit a redox signal within the growth cone, when integrins meet the extracellular matrix [52].

Indeed, the results show that PKG1 needs to be redox-activated to be fully active in the growth cone because primary DRG neurons of redox-dead Cys42Ser PKG1 mutant mice showed enhanced outgrowth and reduced collapse, similar to PKG1 deficient neurons. Integrins and semaphorin 3a (Sema3a) appear to be a major trigger of redox signals in the growth cones [40,53]. In addition, Nadhp oxidases [54] and mitochondria locally modulate ROS signaling in the distal neurite and growth cone, and regulate the direction and the rate of neurite growth [55]. Using dimedone we were able to visualize such redox signals in growing cones, where PKG1 was colocalized with F-actin, and upon collapse, PKG1 redistributed from the tip suggesting a redox-dependent traffic that may direct PKG1 to its diverse phosphorylation targets. Other prominent oxidation targets at the growth cones and branching points are F-actin itself [39], MICAL [56] and collapsin response mediator proteins [40]. Hence, PKG1/cofilin and MICAL/CRMP2 and F-actin confer redox sensitivity to axon guidance [56,57] and likely act in concert.

A number of studies using PKG1 activators and inhibitors have shown that PKG1 is an effector of Sema3a evoked growth cone collapse [58], but the opposite i.e. antagonism of this repulsion signal was also reported [42] and one study suggested that the outcome may depend on the polarization of the neuronal membrane [59]. PKG1 was also found to act downstream of Ephrin- and Slit- mediated repulsion signals [60,61] but PKG1 also acted downstream of p53-mediated growth cone extension [42]. It has to be considered that neurite and axon elongation are contributed by shaft stretching [62], which was not specifically addressed and may contribute to the controversy. PKG1 activators and inhibitors used in most studies are cGMP analogs, which more or less also activate or inhibit other cGMP targets including cyclic

nucleotide gated ion channels and phosphodiesterases. The latter affects cAMP metabolism, which complicates the interpretation because cyclic nucleotides per se are regulators of growth cone attraction and collapse [63,64]. Given the controversy, it is well conceivable that both mechanisms – Npr/cGMP/PKG1 mediated attraction and redox-PKG1 mediated repulsion – cooperate in alternating cycles. One may

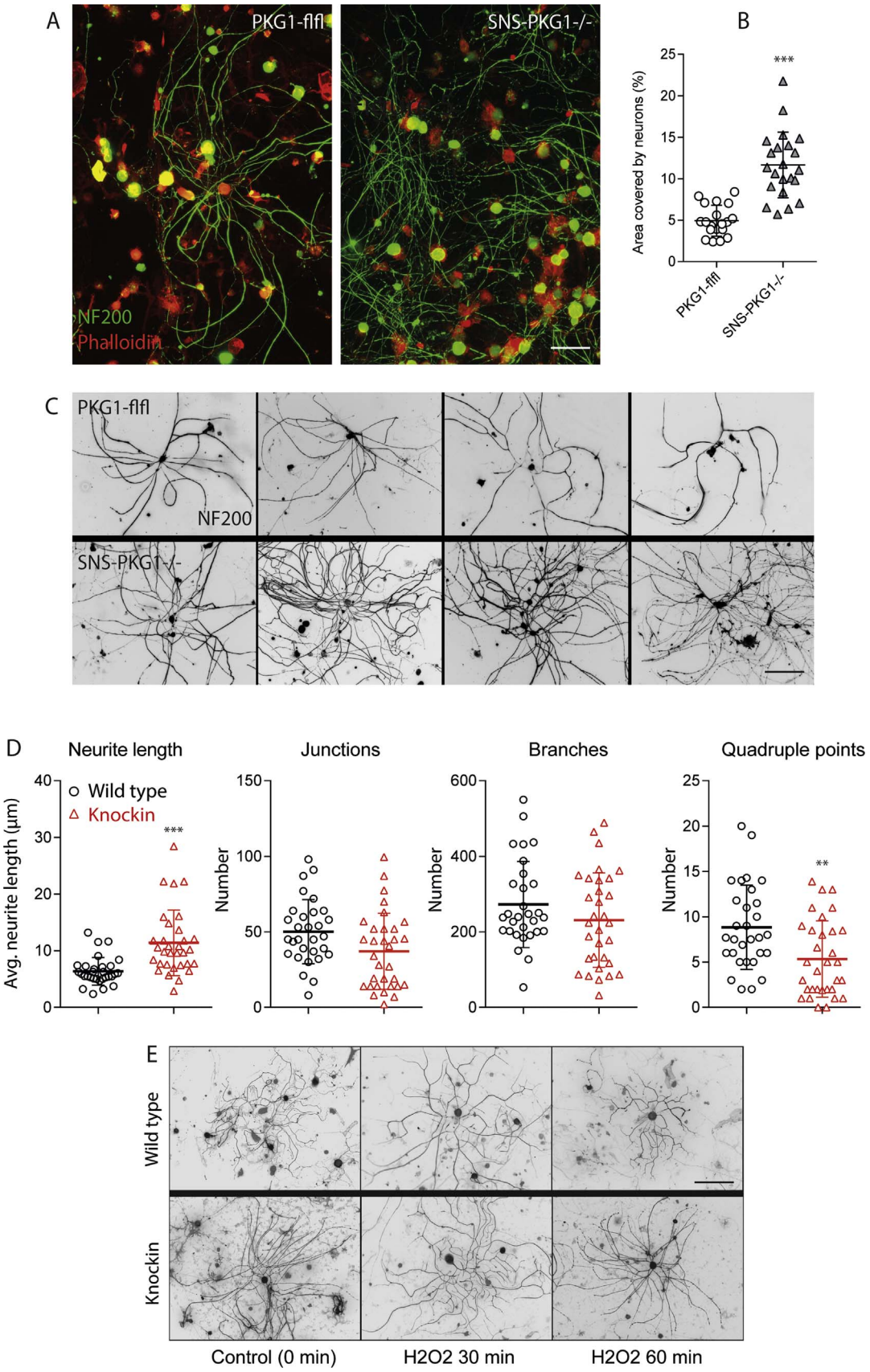

Fig. 6. Immunofluorescence analysis of outgrowth in primary sensory neurons of the dorsal root ganglia of adult PKG1 deficient versus control mice and of Cys42Ser PKG1 redox dead mutant versus wild type mice. A: representative images of DRG cultures stained with neurofilament of 200 kDa (NF200) at 48 h. Phalloidin-Alexa594 counter staining of F-actin was used to assess supporting astrocytes. B: quantification of the area covered with NF200 positive neurons including soma and neurites. Six cultures and 3 images per culture were analyzed. Unpaired, 2-tailed T-test *P < 0.05. C: examples of individual NF200 positive neurons at 48 h. Neurons of SNS-PKG1$^{-/-}$ had more neurites per growing neuron. Scale bar 100 µm. D: scatter plots showing the quantitative analysis of neurite outgrowth and branching in Cys42Ser PKG1 redox dead mutant versus wild type mice 48 h after plating using the segmentation plugin of FIJI. After background subtraction the green NF200 channel was converted to a binary image and then submitted to segmentation analysis. Each scatter represents one image, which were obtained from 9 to 12 slice cultures per genotype. Total neurite length and quadruple points differed significantly between genotypes (2-tailed, unpaired Student's *t*-test, *** P < 0.001, ** P < 0.01. Junctions and branching points were not significant. E: examples of individual NF200 positive neurons of Cys42Ser PKG1 redox dead mutant versus wild type neurons at 48 h after plating. The short exposure to H_2O_2 did not affect the neurite tree. Therefore, all conditions were summarized for quantification (in D). Scale bar 100 µm. A larger panel of images for each condition is presented in Suppl. Fig. 3. (For interpretation of the references to color in this figure legend, the reader is referred to the web version of this article.)

wonder how PKG1, once activated, would "know" what to do. Possibly, it is a matter of site, preferred phosphorylation target and concomitant second messengers including other kinases [65–67] and calcium [68], which ultimately decide the outcome.

Hence, although we focused here on the redox-dependent PKG1-mediated collapse, neuropeptide evoked PKG1 activation leading to attraction may be equally important for axonal path-finding after injury *in vivo*. This idea is supported by previous developmental studies, in which PKG1, activated via the natriuretic peptide pathway, was crucial for axon guidance during critical periods of neuronal development [69,70]. Irrespective of the upstream signaling path, the *in vivo* outcome of PKG1 deficiency in primary afferent neurons was a loss of path-finding, and importantly this leads to heightened neuropathic pain in adult mice.

In line with previous studies, SNS-PKG1$^{-/-}$ mice had a moderate reduction of baseline nociception [9] but they lost this advantage after nerve injury. The result was unexpected, because PKG1 is a major effector of central sensitization in inflammatory nociceptive models [17,18], in part via regulation of spinal mechanisms of 'pain-memory' i.e. nociceptive long term potentiation [9,11]. In contrast to inflammation, nerve injury caused a decrease of PKG1 dimerization and activity suggesting a loss-of-function specific for nerve injury. Based on the *in vitro* results, one may expect that the loss of PKG1 would enhance sprouting of injured or neighboring axons leading to aberrant innervation, hyperexcitability and extension of receptive fields [5,71]. Hence, although PKG1 drives spinal nociceptive LTP it is also crucial for guided axon regrowth so that PKG1 inhibition – although quite effective for the treatment of inflammatory pain – would not prevent or attenuate neuropathic pain after nerve injury.

A recent study using the redox-dead PKG1 mutant mice in behavioral experiments appears to contradict this hypothesis, because the mutants showed weaker nociceptive responses after nerve injury than the controls [21]. However, the PKG1 mutation is not specific for any site or cell [20], hence affecting all PKG1 expressing neurons including sympathetic neurons and vascular cells, so that these mice rather mimic a weak general knockout, or mice under PKG1-inhibitor treatment. Therefore, we used these mice only for *in vitro* studies of primary DRG neurons, in which the redox-dead PKG1 mutant neurons were similar to the SNS-PKG$^{-/-}$ neurons in terms of growth cone collapse, albeit the phenotype was somewhat weaker.

In summary, we show that PKG1 mediates redox-sensitive growth cone collapse, which is required for axon guidance and regeneration

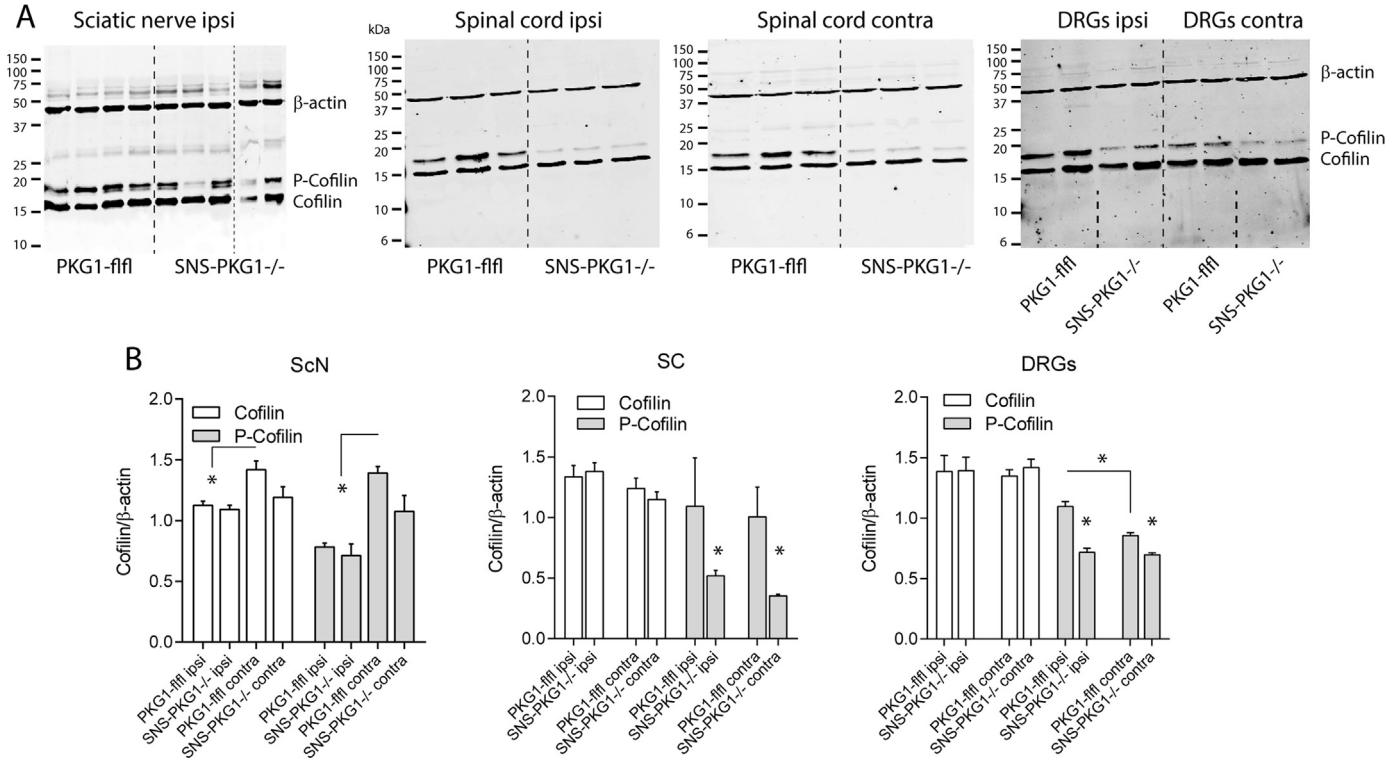

Fig. 7. Western blot analysis of cofilin phosphorylation in the DRGs, spinal cord and crushed sciatic nerve in PKG1^{flfl} and SNS-PKG1$^{-/-}$ mice 28 days after the injury. A: representative blots of the sciatic nerve, spinal cord and DRGs. β-actin was used as loading control. The images are overlays of sequentially developed blots using different IRDyes. B: quantitative Western blot results. The bands of cofilin and phosphorylated cofilin (*p*-cofilin) were normalized to the loading control β-actin. Results of 4–5 mice per genotype, for the DRGs each 2 mice were pooled. Asterisks indicate significant differences with P < 0.05.

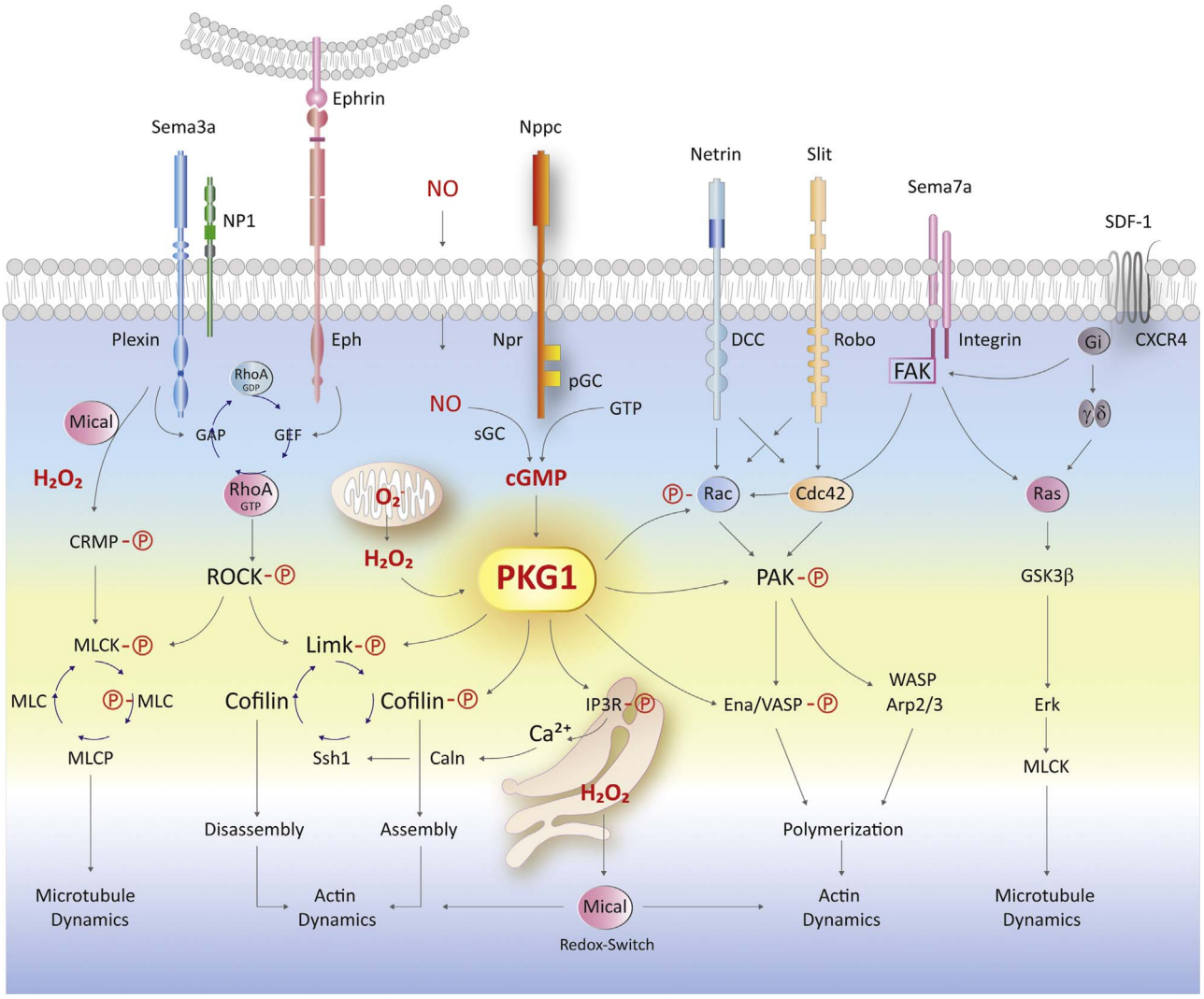

Fig. 8. Illustration of the functions of PKG1 in the context of axonal growth and pathfinding. Protein kinase G (PKG1) is activated by oxidation and dimerization or by cGMP, which is either produced by soluble guanylyl cyclase (sGC) or by natriuretic peptide receptors (Npr). Oxidation-mediated activation of PKG1 is independent of cGMP. Once activated, PKG1 phosphorylates several targets which contribute to the regulation of actin and actin-myosin dynamics including Rho kinase (ROCK), p21 activated kinase (PAK), Lim kinase (LIMK), cofilin, Ena/Vasp proteins, myosin light chain (MLC) and myosin light chain kinase (MLCK). In addition, it phosphorylates the inositol-3-phosphate receptor (IP3R), which is the gate keeper of intracellular calcium stores. In DRG neurons, PKG1 activation causes intracellular calcium release. The effector molecules are all involved in the translation of repulsion and attraction cues into directional axonal growth and neuron migration. The stimuli include semaphorins, netrins, slits, ephrin ligands, natriuretic peptides, chemokines and matrix molecules and their respective receptors. PKG1 is therefore strategically positioned to modify the downstream effects of these stimuli. Particularly, the repulsive cue, semaphorin 3a signals via activation of MICAL, generation of signaling ROS and oxidation-dependent activation of collapsin response mediator proteins (CRMP), which regulate tubulin dynamics. Oxidation-dependent activation of PKG1 followed by cofilin phosphorylation likely represents a complimentary path regulating actin dynamics. By modifying cofilin mediated actin polymerization and depolymerization PKG1 is crucial for guidance of regenerating axons after peripheral nerve injury, which is a prerequisite for correct re-innervation and resolution of chronic neuropathic pain. Abbreviations are the gene names. Gene names and functions are summarized in Suppl. Table 3.

after peripheral nerve injury in mice. Based on previous studies and our results we propose that PKG1 is activated *in vivo* via redox signals originating within the neurons and possibly also by natriuretic peptides. The first likely promotes growth cone repulsion, the latter possibly attraction and the interplay is crucial for proper PKG1 mediated regulation of actin dynamics and axon guidance. The pro-regenerative properties of PKG1 outweigh its pro-nociceptive signaling effects in the spinal cord and therefore, translated to humans, PKG1 inhibition after nerve injury would likely interfere with endogenous repair mechanisms and unfavorably affect the long-term outcome of neuropathic pain.

Author contributions

LV and AH performed experiments, took care of mouse line maintenance and analyzed data. SD and KS performed experiments, analyzed data and provided technical advice. PE provided redox-dead PKG1 mice. IT initiated and organized the study, performed experiments, analyzed data, made the figures and wrote the manuscript.

Acknowledgements

We acknowledge the financial support of the Deutsche Forschungsgemeinschaft (SFB815 A12 to IT, A01 to KS, A02 to SD and CRC1080 A9 to IT). We thank Sabine Harenkamp and Ilka Siebels for technical assistance, Rohini Kuner for SNScre mice, Robert Feil for PKG1-flfl mice. The authors have no conflicts of interest.

Appendix A. Supplementary material

Supplementary data associated with this article can be found in the online version at http://dx.doi.org/10.1016/j.redox.2016.12.004.

References

[1] R.J. Giger, E.R., 2nd Hollis, M.H. Tuszynski, Guidance molecules in axon regeneration, Cold Spring Harb. Perspect. Biol. 2 (2010) a001867.
[2] S. Shim, G.L. Ming, Roles of channels and receptors in the growth cone during PNS axonal regeneration, Exp. Neurol. 223 (2010) 38–44.
[3] W.S. Kingery, J.D. Lu, J.A. Roffers, D.R. Kell, The resolution of neuropathic hyperalgesia following motor and sensory functional recovery in sciatic axonotmetic mononeuropathies, Pain 58 (1994) 157–168.
[4] C.J. Woolf, P. Shortland, R.E. Coggeshall, Peripheral nerve injury triggers central sprouting of myelinated afferents, Nature 355 (1992) 75–78.
[5] S. Cobianchi, J. de Cruz, X. Navarro, Assessment of sensory thresholds and nociceptive fiber growth after sciatic nerve injury reveals the differential contribution of collateral reinnervation and nerve regeneration to neuropathic pain, Exp. Neurol. 255 (2014) 1–11.
[6] B. Hartmann, S. Ahmadi, P.A. Heppenstall, G.R. Lewin, C. Schott, T. Borchardt, P.H. Seeburg, H.U. Zeilhofer, R. Sprengel, R. Kuner, The AMPA receptor subunits GluR-A and GluR-B reciprocally modulate spinal synaptic plasticity and inflammatory pain, Neuron 44 (2004) 637–650.
[7] X. Navarro, M. Vivo, A. Valero-Cabre, Neural plasticity after peripheral nerve injury and regeneration, Prog. Neurobiol. 82 (2007) 163–201.
[8] J. Scholz, D.C. Broom, D.H. Youn, C.D. Mills, T. Kohno, M.R. Suter, K.A. Moore, I. Decosterd, R.E. Coggeshall, C.J. Woolf, Blocking caspase activity prevents transsynaptic neuronal apoptosis and the loss of inhibition in lamina II of the dorsal horn after peripheral nerve injury, J. Neurosci. 25 (2005) 7317–7323.
[9] C. Luo, V. Gangadharan, K.K. Bali, R.G. Xie, N. Agarwal, M. Kurejova, A. Tappe-Theodor, I. Tegeder, S. Feil, G. Lewin, E. Polgar, A.J. Todd, J. Schlossmann, F. Hofmann, D.L. Liu, S.J. Hu, R. Feil, T. Kuner, R. Kuner, Presynaptically localized cyclic GMP-dependent protein kinase 1 Is a key determinant of spinal synaptic potentiation and pain hypersensitivity, PloS Biol. 10 (2012) e1001283.
[10] M. Randic, M.C. Jiang, R. Cerne, Long-term potentiation and long-term depression of primary afferent neurotransmission in the rat spinal cord, J. Neurosci. 13 (1993) 5228–5241.
[11] M.R. Lewin, E.T. Walters, Cyclic GMP pathway is critical for inducing long-term sensitization of nociceptive sensory neurons, Nat. Neurosci. 2 (1999) 18–23.
[12] S. Heine, S. Michalakis, W. Kallenborn-Gerhardt, R. Lu, H.Y. Lim, J. Weiland, D. Del Turco, T. Deller, I. Tegeder, M. Biel, G. Geisslinger, A. Schmidtko, CNGA3: a target of spinal nitric oxide/cGMP signaling and modulator of inflammatory pain hypersensitivity, J. Neurosci. 31 (2011) 11184–11192.
[13] A. Neitz, E. Mergia, U.T. Eysel, D. Koesling, T. Mittmann, Presynaptic nitric oxide/cGMP facilitates glutamate release via hyperpolarization-activated cyclic nucleotide-gated channels in the hippocampus, Eur. J. Neurosci. 33 (2011) 1611–1621.
[14] R. Feil, T. Kleppisch, NO/cGMP-dependent modulation of synaptic transmission, Handb. Exp. Pharmacol. (2008) 529–560. http://dx.doi.org/10.1007/978-3-540-74805-2_16.
[15] T. Kleppisch, R. Feil, CGMP signalling in the mammalian brain: role in synaptic plasticity and behaviour, Handb. Exp. Pharmacol. (2009) 549–579. http://dx.doi.org/10.1007/978-3-540-68964-5_24.
[16] A. Schmidtko, W. Gao, P. Konig, S. Heine, R. Motterlini, P. Ruth, J. Schlossmann, D. Koesling, E. Niederberger, I. Tegeder, A. Friebe, G. Geisslinger, cGMP produced by NO-sensitive guanylyl cyclase essentially contributes to inflammatory and neuropathic pain by using targets different from cGMP-dependent protein kinase I, J. Neurosci. 28 (2008) 8568–8576.
[17] I. Tegeder, D. Del Turco, A. Schmidtko, M. Sausbier, R. Feil, F. Hofmann, T. Deller, P. Ruth, G. Geisslinger, Reduced inflammatory hyperalgesia with preservation of acute thermal nociception in mice lacking cGMP-dependent protein kinase I, Proc. Natl. Acad. Sci. Usa. 101 (2004) 3253–3257.
[18] A. Schmidtko, P. Ruth, G. Geisslinger, I. Tegeder, Inhibition of cyclic guanosine 5′-monophosphate-dependent protein kinase I (PKG-I) in lumbar spinal cord reduces formalin-induced hyperalgesia and PKG upregulation, Nitric Oxide. 8 (2003) 89–94.
[19] T. Kleppisch, W. Wolfsgruber, S. Feil, R. Allmann, C.T. Wotjak, S. Goebbels, K.A. Nave, F. Hofmann, R. Feil, Hippocampal cGMP-dependent protein kinase I supports an age- and protein synthesis-dependent component of long-term potentiation but is not essential for spatial reference and contextual memory, J. Neurosci. 23 (2003) 6005–6012.
[20] J.R. Burgoyne, M. Madhani, F. Cuello, R.L. Charles, J.P. Brennan, E. Schroder, D.D. Browning, P. Eaton, Cysteine redox sensor in PKGIa enables oxidant-induced activation, Science 317 (2007) 1393–1397.
[21] J.E. Lorenz, W. Kallenborn-Gerhardt, R. Lu, K.M. Syhr, P. Eaton, G. Geisslinger, A. Schmidtko, Oxidant-induced activation of cGMP-dependent protein kinase Ialpha mediates neuropathic pain after peripheral nerve injury, Antioxid. Redox Signal. 21 (2014) 1504–1515.
[22] J. Schlossmann, A. Ammendola, K. Ashman, X. Zong, A. Huber, G. Neubauer, G.X. Wang, H.D. Allescher, M. Korth, M. Wilm, F. Hofmann, P. Ruth, Regulation of intracellular calcium by a signalling complex of IRAG, IP3 receptor and cGMP kinase Ibeta, Nature 404 (2000) 197–201.
[23] A. Sporbert, K. Mertsch, A. Smolenski, R.F. Haseloff, G. Schonfelder, M. Paul, P. Ruth, U. Walter, I.E. Blasig, Phosphorylation of vasodilator-stimulated phosphoprotein: a consequence of nitric oxide- and cGMP-mediated signal transduction in brain capillary endothelial cells and astrocytes, Brain Res. Mol. Brain Res. 67 (1999) 258–266.
[24] C.R. Sunico, D. Gonzalez-Forero, G. Dominguez, J.M. Garcia-Verdugo, B. Moreno-Lopez, Nitric oxide induces pathological synapse loss by a protein kinase G-, Rho kinase-dependent mechanism preceded by myosin light chain phosphorylation, J. Neurosci. 30 (2010) 973–984.
[25] V. Bockhart, C.E. Constantin, A. Haussler, N. Wijnvoord, M. Kanngiesser, T. Myrczek, G. Pickert, L. Popp, J.M. Sobotzik, M. Pasparakis, R. Kuner, G. Geisslinger, C. Schultz, M. Kress, I. Tegeder, Inhibitor kappaB Kinase beta deficiency in primary nociceptive neurons increases TRP channel sensitivity, J. Neurosci. 29 (2009) 12919–12929.
[26] N. Agarwal, S. Offermanns, R. Kuner, Conditional gene deletion in primary nociceptive neurons of trigeminal ganglia and dorsal root ganglia, Genesis 38 (2004) 122–129.
[27] N. Agarwal, P. Pacher, I. Tegeder, F. Amaya, C.E. Constantin, G.J. Brenner, T. Rubino, C.W. Michalski, G. Marsicano, K. Monory, K. Mackie, C. Marian, S. Batkai, D. Parolaro, M.J. Fischer, P. Reeh, G. Kunos, M. Kress, B. Lutz, C.J. Woolf, R. Kuner, Cannabinoids mediate analgesia largely via peripheral type 1 cannabinoid receptors in nociceptors, Nat. Neurosci. 10 (2007) 870–879.
[28] P. Young, L. Qiu, D. Wang, S. Zhao, J. Gross, G. Feng, Single-neuron labeling with inducible Cre-mediated knockout in transgenic mice, Nat. Neurosci. 11 (2008) 721–728.
[29] M. Kanngiesser, N. Mair, H.Y. Lim, K. Zschiebsch, J. Blees, A. Haussler, B. Brune, N. Ferreiros, M. Kress, I. Tegeder, Hypoxia-inducible factor 1 regulates heat and cold pain sensitivity and persistence, Antioxid. Redox Signal. 20 (2014) 2555–2571.
[30] I. Decosterd, C.J. Woolf, Spared nerve injury: an animal model of persistent peripheral neuropathic pain, Pain 87 (2000) 149–158.
[31] I. Tegeder, M. Costigan, R.S. Griffin, A. Abele, I. Belfer, H. Schmidt, C. Ehnert, J. Nejim, C. Marian, J. Scholz, T. Wu, A. Allchorne, L. Diatchenko, A.M. Binshtok, D. Goldman, J. Adolph, S. Sama, S.J. Atlas, W.A. Carlezon, A. Parsegian, J. Lotsch, R.B. Fillingim, W. Maixner, G. Geisslinger, M.B. Max, C.J. Woolf, GTP cyclohydrolase and tetrahydrobiopterin regulate pain sensitivity and persistence, Nat. Med. 12 (2006) 1269–1277.
[32] W. Tetzlaff, H. Zwiers, K. Lederis, L. Cassar, M.A. Bisby, Axonal transport and localization of B-50/gap-43-like immunoreactivity in regenerating sciatic and facial nerves of the rat, J. Neurosci. 9 (1989) 1303–1313.
[33] K.W. Dunn, M.M. Kamocka, J.H. McDonald, A practical guide to evaluating colocalization in biological microscopy, Am. J. Physiol. Cell Physiol. 300 (2011) C723–C742.
[34] S. Bolte, F.P. Cordelieres, A guided tour into subcellular colocalization analysis in light microscopy, J. Microsc. 224 (2006) 213–232.
[35] L.B. Poole, C. Klomsiri, S.A. Knaggs, C.M. Furdui, K.J. Nelson, M.J. Thomas, J.S. Fetrow, L.W. Daniel, S.B. King, Fluorescent and affinity-based tools to detect cysteine sulfenic acid formation in proteins, Bioconjug Chem. 18 (2007) 2004–2017.
[36] L. Valek, M. Kanngiesser, A. Haussler, N. Agarwal, C.H. Lillig, I. Tegeder, Redoxins in peripheral neurons after sciatic nerve injury, Free Radic. Biol. Med. 89 (2015) 581–592.
[37] A.T. Saurin, H. Neubert, J.P. Brennan, P. Eaton, Widespread sulfenic acid formation in tissues in response to hydrogen peroxide, Proc. Natl. Acad. Sci. USA 101 (2004) 17982–17987.
[38] B.W. Bernstein, J.R. Bamburg, Neuronal guidance: a redox signal involving Mical, Curr. Biol. 20 (2010) R360–R362.
[39] R.J. Hung, C.W. Pak, J.R. Terman, Direct redox regulation of F-actin assembly and disassembly by Mical, Science 334 (2011) 1710–1713.
[40] A. Morinaka, M. Yamada, R. Itofusa, Y. Funato, Y. Yoshimura, F. Nakamura, T. Yoshimura, K. Kaibuchi, Y. Goshima, M. Hoshino, H. Kamiguchi, H. Miki, Thioredoxin mediates oxidation-dependent phosphorylation of CRMP2 and growth cone collapse, Sci. Signal. (2011) 4.
[41] M. Gellert, S. Venz, J. Mitlohner, C. Cott, E.M. Hanschmann, C.H. Lillig, Identification of a dithiol-disulfide switch in collapsin response mediator protein 2 (CRMP2) that is toggled in a model of neuronal differentiation, J. Biol. Chem. 288 (2013) 35117–35125.
[42] A. Tedeschi, T. Nguyen, S.U. Steele, S. Feil, U. Naumann, R. Feil, S. Di Giovanni, The tumor suppressor p53 transcriptionally regulates cGKI expression during neuronal maturation and is required for cGMP-dependent growth cone collapse, J. Neurosci. 29 (2009) 15155–15160.
[43] E.W. Dent, S.L. Gupton, F.B. Gertler, The growth cone cytoskeleton in axon outgrowth and guidance, Cold Spring Harb. Perspect. Biol. 3 (3) (2011) a001800 (001810.001101/cshperspect.a001800).
[44] H. Aizawa, S. Wakatsuki, A. Ishii, K. Moriyama, Y. Sasaki, K. Ohashi, Y. Sekine-Aizawa, A. Sehara-Fujisawa, K. Mizuno, Y. Goshima, I. Yahara, Phosphorylation of cofilin by LIM-kinase is necessary for semaphorin 3A-induced growth cone collapse, Nat. Neurosci. 4 (2001) 367–373.
[45] M. Endo, K. Ohashi, Y. Sasaki, Y. Goshima, R. Niwa, T. Uemura, K. Mizuno, Control of growth cone motility and morphology by LIM kinase and Slingshot via phosphorylation and dephosphorylation of cofilin, J. Neurosci. 23 (2003) 2527–2537.
[46] S.L. Lindsay, S. Ramsey, M. Aitchison, T. Renne, T.J. Evans, Modulation of lamellipodial structure and dynamics by NO-dependent phosphorylation of VASP Ser239, J. Cell Sci. 120 (2007) 3011–3021.
[47] H.G. Wang, F.M. Lu, I. Jin, H. Udo, E.R. Kandel, J. de Vente, U. Walter, S.M. Lohmann, R.D. Hawkins, I. Antonova, Presynaptic and postsynaptic roles of NO, cGK, and RhoA in long-lasting potentiation and aggregation of synaptic proteins, Neuron 45 (2005) 389–403.
[48] S. Arber, F.A. Barbayannis, H. Hanser, C. Schneider, C.A. Stanyon, O. Bernard, P. Caroni, Regulation of actin dynamics through phosphorylation of cofilin by LIM-kinase, Nature 393 (1998) 805–809.
[49] P.J. Meberg, Signal-regulated ADF/cofilin activity and growth cone motility, Mol. Neurobiol. 21 (2000) 97–107.

[50] S. Mandal, A. Stanco, E.S. Buys, G. Enikolopov, J.L. Rubenstein, Soluble guanylate cyclase generation of cGMP regulates migration of MGE neurons, J. Neurosci. 33 (2013) 16897–16914.
[51] Y. Hou, R.D. Ye, D.D. Browning, Activation of the small GTPase Rac1 by cGMP-dependent protein kinase, Cell Signal. 16 (2004) 1061–1069.
[52] J.A. Eble, F.F. de Rezende, Redox-relevant aspects of the extracellular matrix and its cellular contacts via integrins, Antioxid. Redox Signal. 20 (2014) 1977–1993.
[53] M.L. Lemons, M.L. Condic, Combined integrin activation and intracellular cAMP cause Rho GTPase dependent growth cone collapse on laminin-1, Exp. Neurol. 202 (2006) 324–335.
[54] V. Munnamalai, C.J. Weaver, C.E. Weisheit, P. Venkatraman, Z.S. Agim, M.T. Quinn, D.M. Suter, Bidirectional interactions between NOX2-type NADPH oxidase and the F-actin cytoskeleton in neuronal growth cones, J. Neurochem. 130 (2014) 526–540.
[55] M.B. Steketee, S.N. Moysidis, J.E. Weinstein, A. Kreymerman, J.P. Silva, S. Iqbal, J.L. Goldberg, Mitochondrial dynamics regulate growth cone motility, guidance, and neurite growth rate in perinatal retinal ganglion cells in vitro, Invest Ophthalmol. Vis. Sci. 53 (2012) 7402–7411.
[56] R.J. Hung, U. Yazdani, J. Yoon, H. Wu, T. Yang, N. Gupta, Z. Huang, W.J. van Berkel, J.R. Terman, Mical links semaphorins to F-actin disassembly, Nature 463 (2010) 823–827.
[57] J.R. Terman, T. Mao, R.J. Pasterkamp, H.H. Yu, A.L. Kolodkin, MICALs, a family of conserved flavoprotein oxidoreductases, function in plexin-mediated axonal repulsion, Cell 109 (2002) 887–900.
[58] V.D. Dontchev, P.C. Letourneau, Growth cones integrate signaling from multiple guidance cues, J. Histochem Cytochem. 51 (2003) 435–444.
[59] M. Nishiyama, M.J. von Schimmelmann, K. Togashi, W.M. Findley, K. Hong, Membrane potential shifts caused by diffusible guidance signals direct growth-cone turning, Nat. Neurosci. 11 (2008) 762–771.
[60] X. Yue, C. Dreyfus, T.A. Kong, R. Zhou, A subset of signal transduction pathways is required for hippocampal growth cone collapse induced by ephrin-A5, Dev. Neurobiol. 68 (2008) 1269–1286.
[61] K.T. Nguyen-Ba-Charvet, K. Brose, V. Marillat, C. Sotelo, M. Tessier-Lavigne, A. Chedotal, Sensory axon response to substrate-bound Slit2 is modulated by laminin and cyclic GMP, Mol. Cell Neurosci. 17 (2001) 1048–1058.
[62] P. Lamoureux, S.R. Heidemann, N.R. Martzke, K.E. Miller, Growth and elongation within and along the axon, Dev. Neurobiol. 70 (2010) 135–149 (110.1002/dneu.20764).
[63] Q. Wang, J.Q. Zheng, CAMP-mediated regulation of neurotrophin-induced collapse of nerve growth cones, J. Neurosci. 18 (1998) 4973–4984.
[64] H. Song, G. Ming, Z. He, M. Lehmann, L. McKerracher, M. Tessier-Lavigne, M. Poo, Conversion of neuronal growth cone responses from repulsion to attraction by cyclic nucleotides, Science 281 (1998) 1515–1518.
[65] N. Mitsui, R. Inatome, S. Takahashi, Y. Goshima, H. Yamamura, S. Yanagi, Involvement of Fes/Fps tyrosine kinase in semaphorin3A signaling, EMBO J. 21 (2002) 3274–3285.
[66] G.R. Buel, J. Rush, B.A. Ballif, Fyn promotes phosphorylation of collapsin response mediator protein 1 at tyrosine 504, a novel, isoform-specific regulatory site, J. Cell Biochem. 111 (2010) 20–28. http://dx.doi.org/10.1002/jcb.22659.
[67] B. Knoll, U. Drescher, Src family kinases are involved in EphA receptor-mediated retinal axon guidance, J. Neurosci. 24 (2004) 6248–6257.
[68] J.Q. Zheng, Turning of nerve growth cones induced by localized increases in intracellular calcium ions, Nature 403 (2000) 89–93.
[69] H. Schmidt, M. Werner, P.A. Heppenstall, M. Henning, M.I. More, S. Kuhbandner, G.R. Lewin, F. Hofmann, R. Feil, F.G. Rathjen, cGMP-mediated signaling via cGKIalpha is required for the guidance and connectivity of sensory axons, J. Cell Biol. 159 (2002) 489–498.
[70] G. Ter-Avetisyan, F.G. Rathjen, H. Schmidt, Bifurcation of axons from cranial sensory neurons is disabled in the absence of Npr2-induced cGMP signaling, J. Neurosci. 34 (2014) 737–747.
[71] J.C. Peleshok, A. Ribeiro-da-Silva, Delayed reinnervation by nonpeptidergic nociceptive afferents of the glabrous skin of the rat hindpaw in a neuropathic pain model, J. Comp. Neurol. 519 (2011) 49–63.